JOURNAL OF GEOPHYSICAL RESEARCH, VOL. 105, NO. B5, PAGES 10,899–10,921, MAY 10, 2000

Three-dimensional seismic model of the Sierra Nevada arc, California, and its implications for crustal and upper mantle composition

Moritz M. Fliedner[1] and Simon L. Klemperer
Department of Geophysics, Stanford University, Stanford, California

Nikolas I. Christensen
Department of Geology and Geophysics, University of Wisconsin, Madison

Abstract. A three-dimensional P wave velocity model of south-central California from the Coast Ranges to the Sierra Nevada shows that the crust under most of the southern Sierra Nevada batholith has seismic velocities (5.9–6.3 km/s) below the continental average. The crust is not much thicker (on average about 35 km) than in the adjacent Great Valley and Basin and Range province apart from a small, northward thickening, crustal root under the western Sierra Nevada that reaches a depth of 42 km. Crustal velocities above the continental average are observed beneath much of the Great Valley due to a high-velocity body underlying the sedimentary basin and the Foothills metamorphic belt (6.4–7.0 km/s). Upper mantle velocities are generally low (7.8 km/s) but span a wide range (7.4–8.2 km/s). We display the velocity model in several cross sections and maps of Moho depth and average crustal velocity. The measured velocities in the upper and mid crust of the Sierra Nevada batholith are in good agreement with laboratory measurements on Sierra Nevada tonalites after corrections for density and temperature. Peridotite xenoliths from the eastern Sierra Nevada suggest strong upper mantle anisotropy, which could explain some of the velocity heterogeneity in the Sierra Nevada mantle. By the time Cretaceous subduction-related magmatism ceased, the Sierra Nevada arc must have had a thick mafic lower crust; yet a principal result of our work is that today the batholith has a crust of mainly felsic composition throughout. A subcrustal layer with velocities below normal P_n velocities (<7.6 km/s) may indicate the presence of lower crustal material in eclogite facies.

1. Introduction

The modern tectonic framework of central California is dominated by the San Andreas strike-slip fault system, but its basic geologic framework is related to its earlier subduction regime, which continues today north of the Mendocino Triple Junction in northern California. The three major geologic provinces of central California, the Coast Ranges, the Great (Central) Valley, and the Sierra Nevada, represent the accretionary-prism complex, the forearc sedimentary basin, and the exhumed batholith of a magmatic arc system generated during Mesozoic subduction, respectively. To the east and south, bounded by the eastern scarp of the Sierra Nevada, and to the south bounded by the Garlock Fault in southern California, lies the extensional Basin and Range province (Figures 1 and 2). Our seismic investigation of the crust from the Pacific coast to the western Basin and Range province was designed to show the structural consequences of this tectonic development.

In summer 1993 the Southern Sierra Nevada Continental Dynamics (SSCD) project shot two seismic refraction lines in central California [*Malin et al.*, 1995; *Wernicke et al.*, 1996]. The first ran from the Coast Ranges across the Sierra Nevada and western Basin and Range province (west-east line, length: 400 km), and the second in Owens Valley east of the Sierra Nevada (north-south line, length: 325 km). In addition, a modified west-east line recorded the NPE (Non-Proliferation Experiment) shot on the Nevada Test Site over a length of 480 km into the Coast Ranges (Figure 2). With a shot spacing of 50 km and a receiver spacing of 500 m this survey is the most detailed active seismic study of the Sierra Nevada batholith to date.

[1]Now at Bullard Laboratories, University of Cambridge, Cambridge, England.

Paper number 2000JB900029.
0148-0227/00/2000JB900029$09.00

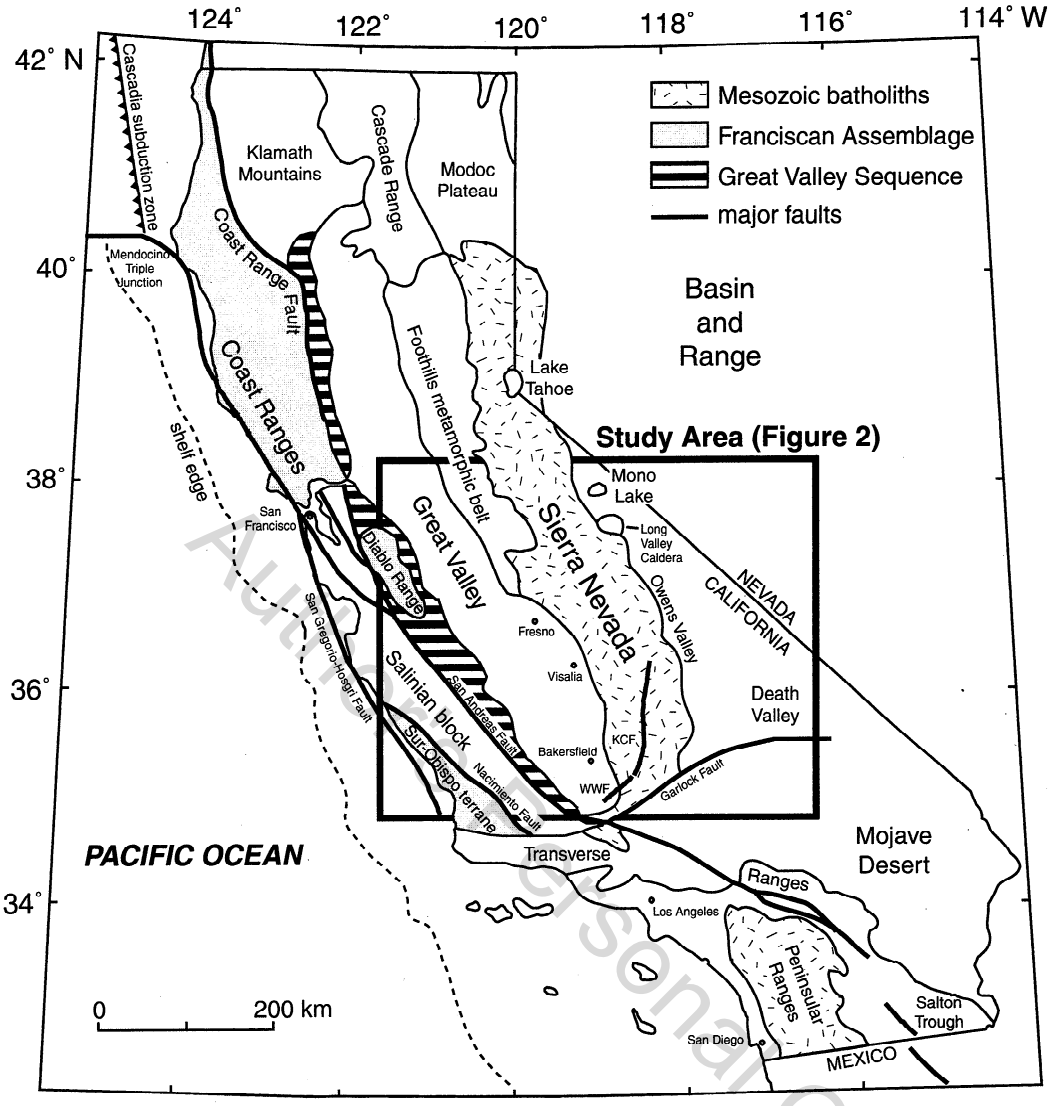

Figure 1. Overview map of California and its tectonic provinces (modified from *Fuis and Mooney* [1990]; and *Saltus and Lachenbruch* [1991]). WWF, White Wolf Fault; KCF, Kern Canyon Fault. The outlined study area is shown in detail in Figure 2.

Analyses of the first arrivals and wide-angle Moho reflections (P_mP) from this data set have been reported by *Fliedner et al.* [1996] and *Ruppert et al.* [1998]. This study expands on the earlier results in several ways. (1) We have modeled a strong secondary crustal refracted arrival in order to resolve the velocity gradient in the lower crust. (2) We remodel some of the older seismic data collected in the region in order to improve the three-dimensional picture of the crust in central California, updating the review by *Mooney and Weaver* [1989]. (3) We present laboratory data on velocities in rocks from the region to better understand crustal and upper mantle composition. We note that the major controversy we resolve, namely, the seismic velocities (and by implication the composition) of the Sierran lower crust, is complicated for the simple reason that is is notoriously difficult to derive accurate lower crustal velocities from surface seismic data.

The additional data sets fall into two groups: (1) previous, densely sampled two- and three-dimensional seismic refraction surveys in the Coast Ranges and Great Valley and (2) a set of earthquake recordings within the Sierra Nevada batholith published by *Savage et al.* [1994] and here referred to as "the earthquake data." We have not included the pioneering data of *Eaton* [1966] and *Carder* [1973], which started the Sierra Nevada controversy, because they are too sparse to be inverted together with the much denser modern data and also because they fall partially outside our study area (their competing models are discussed with regard to the SSCD data of *Fliedner et al.* [1996]). Most of the refraction data have been analyzed and published before [*Colburn and Walter,* 1984; *Murphy and Walter,* 1984; *Colburn and Mooney,* 1986; *Holbrook and Mooney,* 1987; *Howie et al.*, 1993].

We compare the seismic observations with laboratory measurements on crustal and mantle rock samples from the same area. Our seismic results imply a silicic composition of the crust in the Sierra Nevada. This supports the conclusion from observations of tonalitic

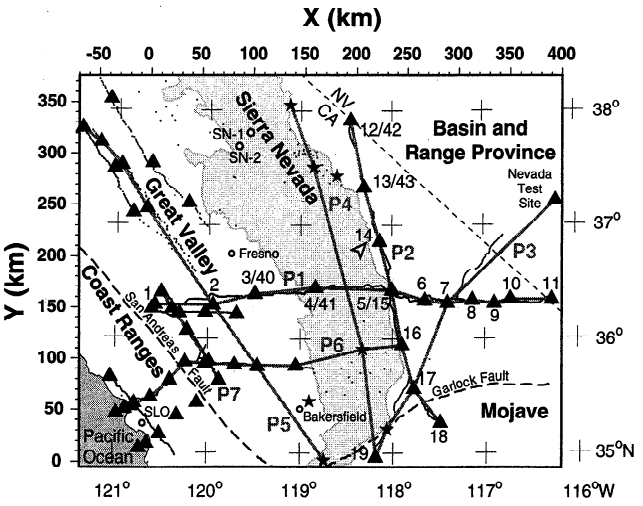

Figure 2. Area covered by 3-D seismic velocity model. Black triangles are shot point locations; numbered shot locations are SSCD: 1–11 west-east line, 12–19 north-south line, and 40–43 fan shots. Stars are earthquake epicenters. Black dots are receiver locations. Gray lines, labeled P1 to P7 are profiles in Plate 1. White circles are locations of tonalite samples SN-1 and SN-2 of Figure 9 and Table 1. Arrow points to Oak Creek, collection site of mantle xenoliths. SLO is San Luis Obispo. The Sierra Nevada batholith is light gray.

lower crustal exposures at the southern end of the Sierra Nevada [*Pickett and Saleeby,* 1993] that the batholith does not become more mafic with depth. The geological evidence for a silicic crust and the consequences for the development of the Sierra Nevada arc have most recently been discussed by *Ducea and Saleeby* [1998a].

The upper crustal structure of the Basin and Range to the east of the Sierra Nevada is discussed in more detail by *Duran* [1997]. This work is also based on the SSCD seismic data. A magnetotelluric survey in the SSCD program [*Park et al.,* 1996] found low electric resistivities in the lower crust and upper mantle of the Sierra Nevada. This is attributed to partial melt at least in the eastern Sierra Nevada.

2. Seismic Data Analysis

We have used the published first-arrival travel times from the data sets of *Colburn and Walter* [1984] and *Murphy and Walter* [1984]; we used our own picks from the original seismic records from the three Great Valley strike lines, of which only two have been published [*Colburn and Mooney,* 1986; *Holbrook and Mooney,* 1987] and the San Luis Obispo 2-D and 3-D data set [see, e.g., *Howie et al.,* 1993]. From the earthquake data set we used those events and stations that fall within our study area as picked by *Savage et al.* [1994].

Although most of the seismic data we discuss are in-line recordings, the use of broadside fan shots from the SSCD data set and the integration of earthquake data and crossing profiles make 3-D analysis possible. For our travel time analysis we use a 3-D tomography algorithm of *Hole* [1992], which computes travel times using a finite difference code based on the method of *Vidale* [1990]. The code is able to handle both first and later arrivals including reflections [*Hole and Zelt,* 1995]. Refracted arrivals (first arrivals of P_g and P_n, and secondary P_g) were inverted for crustal and upper mantle velocities, and the Moho reflection P_mP was inverted for the location of the reflector [*Hole et al.,* 1992] and lower crustal velocities [*Zelt et al.,* 1996]. The reflection Moho was used to enforce a velocity discontinuity between crust and mantle in order to trace P_n more realistically: a pure refraction inversion would smooth out the crust-mantle transition over that part of the lower crust which is unconstrained by turning rays.

In Figure 3, we display six shot gathers from the SSCD data set. The NPE recording (Figure 3a; reduced at 8 km/s) shows P_n as a clear first arrival from 170 km offset to the end of the line at over 450 km offset (note the delay due to Great Valley sediments in the offset range of 300 to 380 km). P_g is a strong secondary arrival out to offsets of about 400 km. The following two records (Figures 3b and 3c) are from the same shot point location in the western foothills of the Sierra Nevada, recorded as in-line shot 4 in the SSCD west-east receiver line and as fan shot 41 in the north-south receiver line. Note the absence of short offsets due to the distance of shot 41 from the receiver line. The in-line record (Figure 3b), shot 4, shows the great difference in quality of later arrivals in the east (Basin and Range) where P_mP is visible from precritical offsets of about 5 km to post-critical offsets at the end of the line, and in the west (Great Valley) where no deep reflections can be picked. The fan record (Figure 3c) shows arrivals from the Sierra Nevada batholith approximately beneath the highest part of the mountain range. P_mP arrives about 1 s later in the north than in the south at equal offsets due to northward deepening of the Moho. The other fan shot (Figure 3e; the in-line recording of the same shot is Figure 3d) was recorded in the west-east line from a shot to the north in Owens Valley. It shows the deepest Moho arrival in the study area (see below). Shots from the Great Valley (e.g., shot 2; Figure 3f) suffer from reverberations within the sedimentary basin (reflected refraction following the first arrival with 3.5 s delay), but show still a recognizable P_n signal and a strong long-offset P_g. Additional data sections are presented by *Fliedner* [1997].

Figure 4 shows five different views of the three-dimensional ray coverage of our velocity model. The first four are views from the side through the transparent model cube: Figures 4a and 4c are views in the Y direction, that is, rays projected along the Y axis into the X-Z plane; Figures 4b anc 4d are views in the X direction, that is, rays projected along the X axis into the Y-Z plane; Figure 4e is an aerial (map) view of the first-arrival ray coverage. High areal coverage is achieved where fan recordings are available (Figure 4e), both in the center of the SSCD data set (X = 100–250 km, Y = 150–250 km) and in the San Luis Obispo area

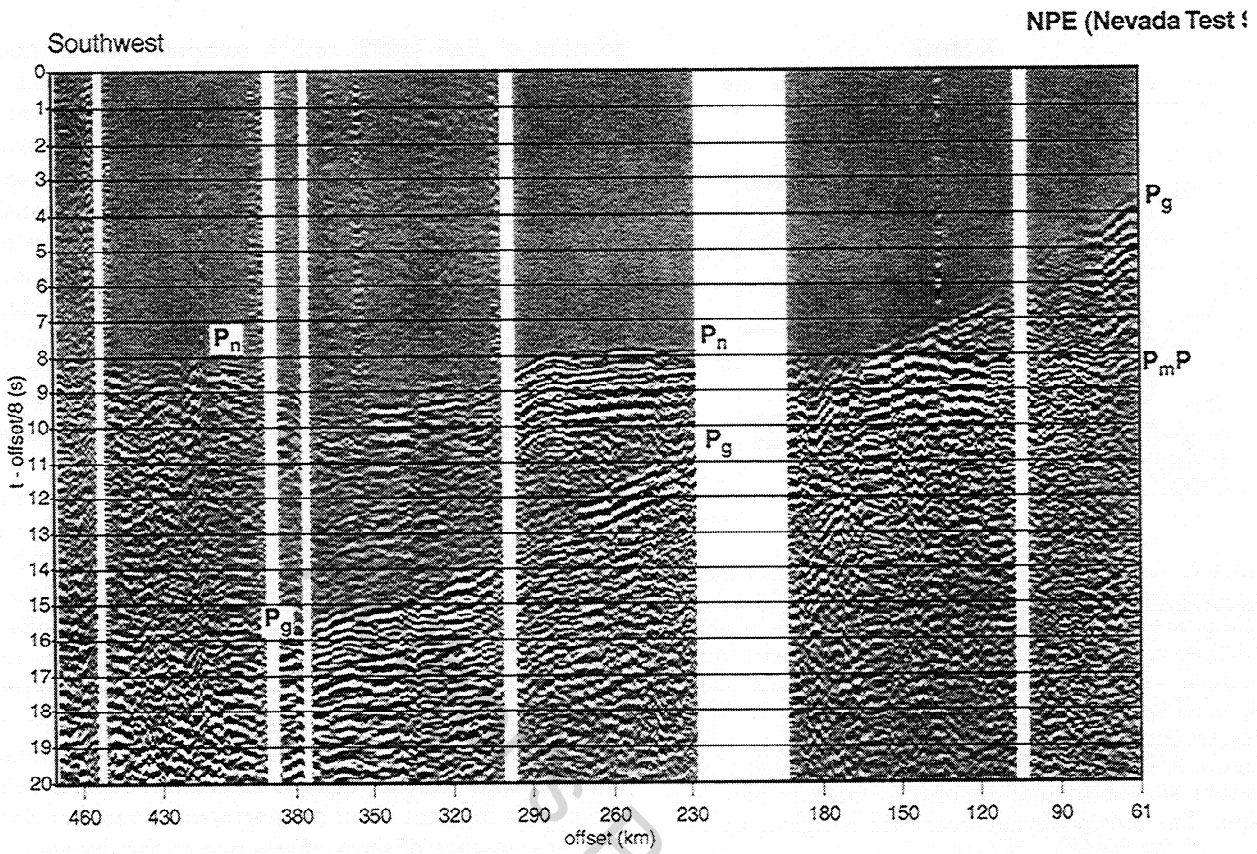

Figure 3a. SSCD gather from NPE shot displayed with travel time reduced at 8 km/s. Shot point location is indicated by inverted triangle.

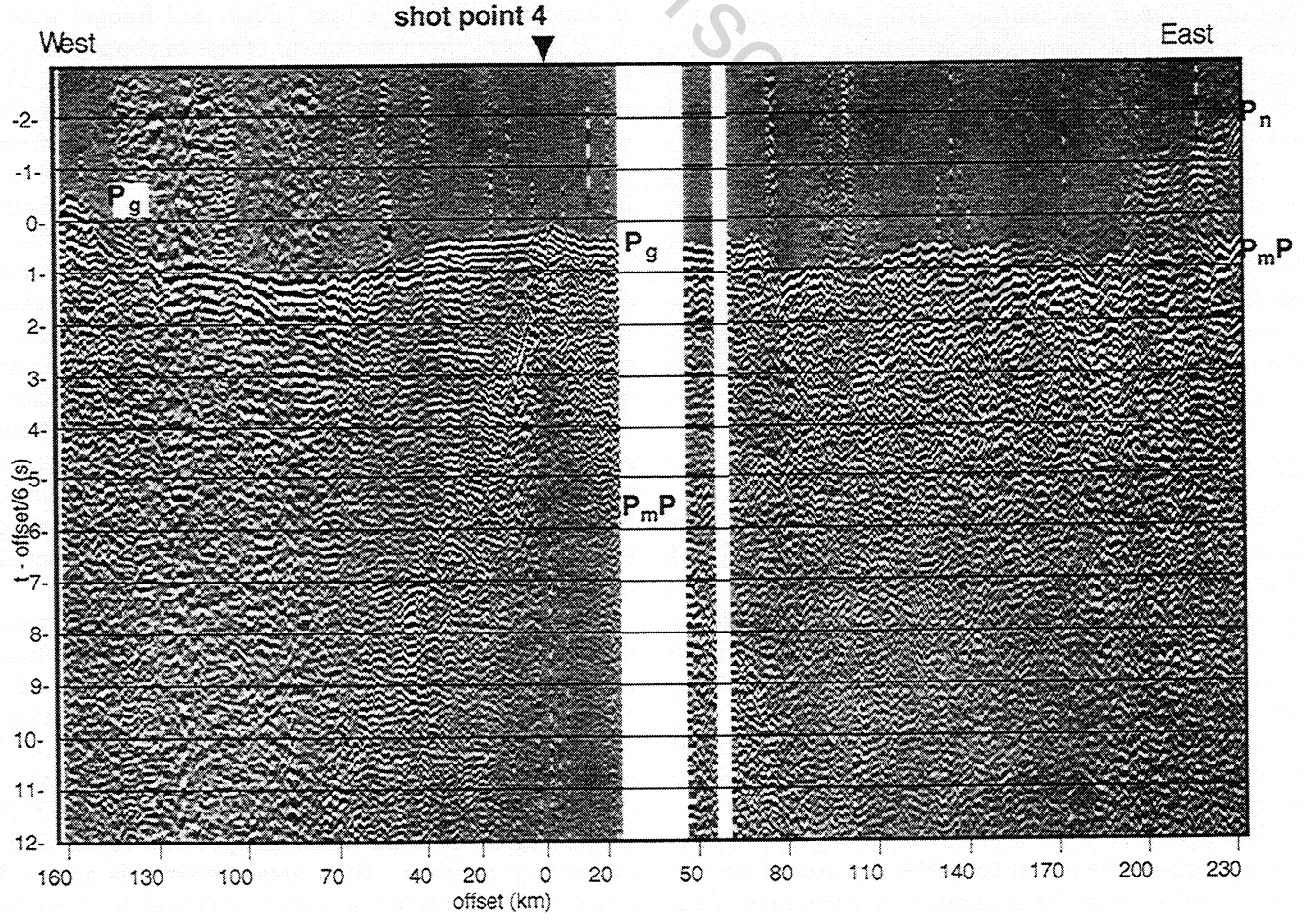

Figure 3b. SSCD gather from shot point 4 displayed with travel time reduced at 6 km/s. Shot point location is indicated by inverted triangle. Shot point 4 is coincident with shot point 41.

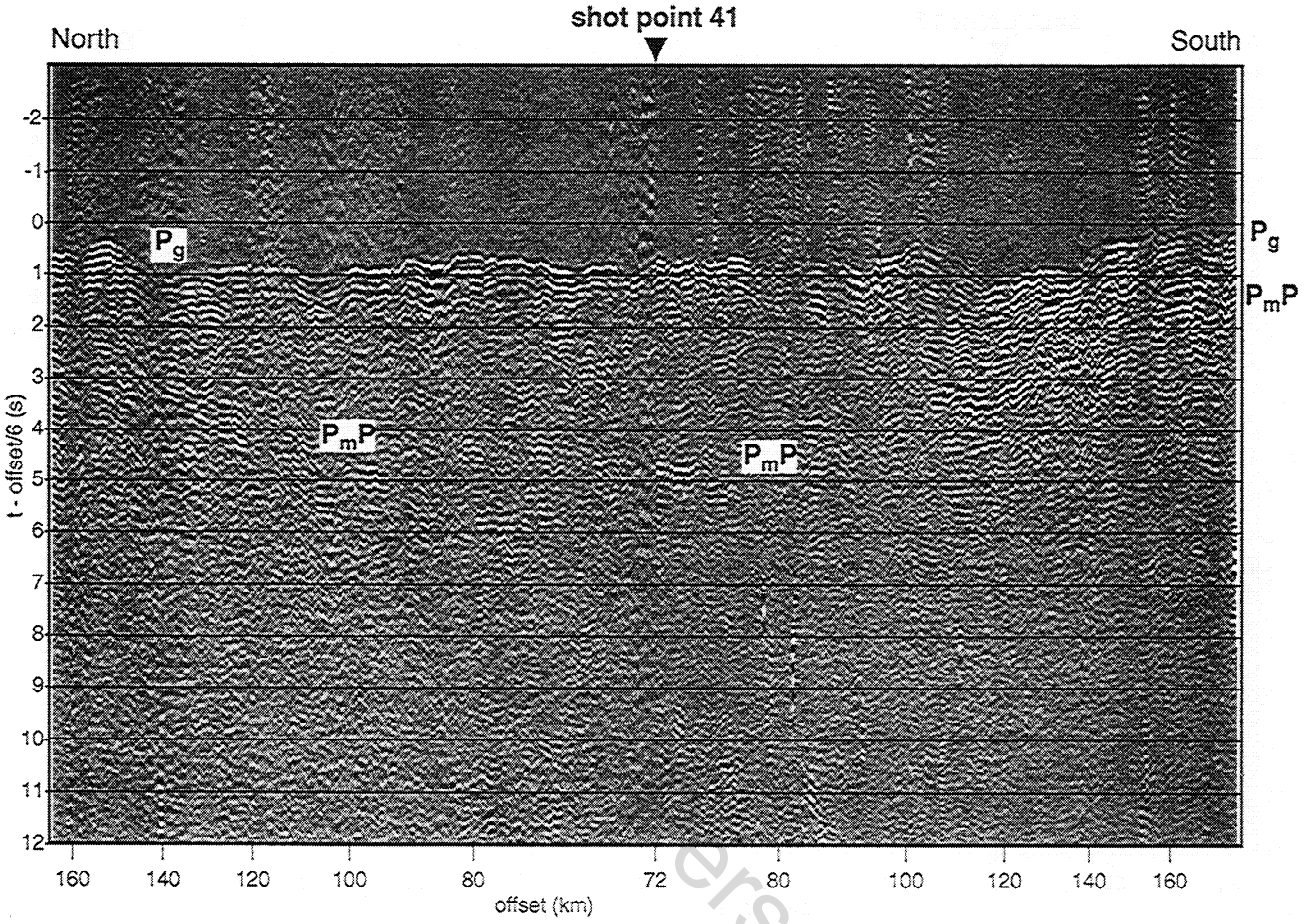

Figure 3c. Same as Figure 3b, except for shot point 41. The inverted triangle marks the projection of the shot point location into the displayed receiver line. Gather is displayed with constant trace spacing (non-linear offset scale).

(around $X = 0$ km, $Y = 50$ km). The other data sets are essentially two dimensional or, in the case of the earthquake data, have only sparse coverage. The upper 15 km of the crust are well covered by P_g first arrivals (Figuress 4a and 4b), as is the region directly beneath the Moho at about 35 km depth where most P_n rays turn. No first arrivals turn in the lower 15 km of the crust. This region is covered by later arrivals, secondary P_g and P_mP (Figures 4c and 4d). P_mP rays are only plotted between the Moho reflector and a mid-crustal transition at 10–15 km depth, the depth range over which P_mP was used for velocity inversion. This transition can be traced in some areas, particularly the Basin and Range, as a reflector [*Ruppert et al.,* 1998; *Duran,* 1997] but is not used otherwise in this study.

The spatial resolution of the velocity model can be tested by inverting travel times calculated from a synthetic model of sinusoidal velocity anomalies (checkerboard test) superimposed on a background model that reflects the general (long wavelength) features of the real model (we use a smoothed version of our velocity model). The degree to which anomalies of different sizes (wavelength of the sinusoid velocity perturbation) can be reconstructed by the inversion gives a qualitative measure of the details that can be resolved with our data set. Figure 5 shows the inversion results of two checkerboards on a section through the SSCD west-east line corresponding with the section of *Ruppert et al.* [1998]. The amplitude of the velocity perturbation is ±0.2 km/s and the anomaly size (half wavelength) is 12.5 km vertically/125 km horizontally in Figure 5a and 7.5 km vertically/62.5 km horizontally in Figure 5b. The long-wavelength anomalies (Figure 5a) are well resolved throughout the crust both in location (except in the deepest part of the crustal root) and amplitude. Smaller amplitudes can only be resolved in the upper crust. The streaking in Figure 5b indicates that the limits in resolving power of the data set have been reached.

An important question is how well the velocity in the lower crust can be constrained. If the velocity gradient in the lower crust is low, there is a wide gap between the turning depths of the first arrivals of P_g and P_n. P_n is not very sensitive to the velocities in the lower crust and for P_mP there is a trade-off between lower crustal velocity and reflector (Moho) depth. The most direct measure, though, is the secondary crustal P_g arrival, which converges at long offsets with the P_mP reflection. The SSCD data show a strong secondary crustal

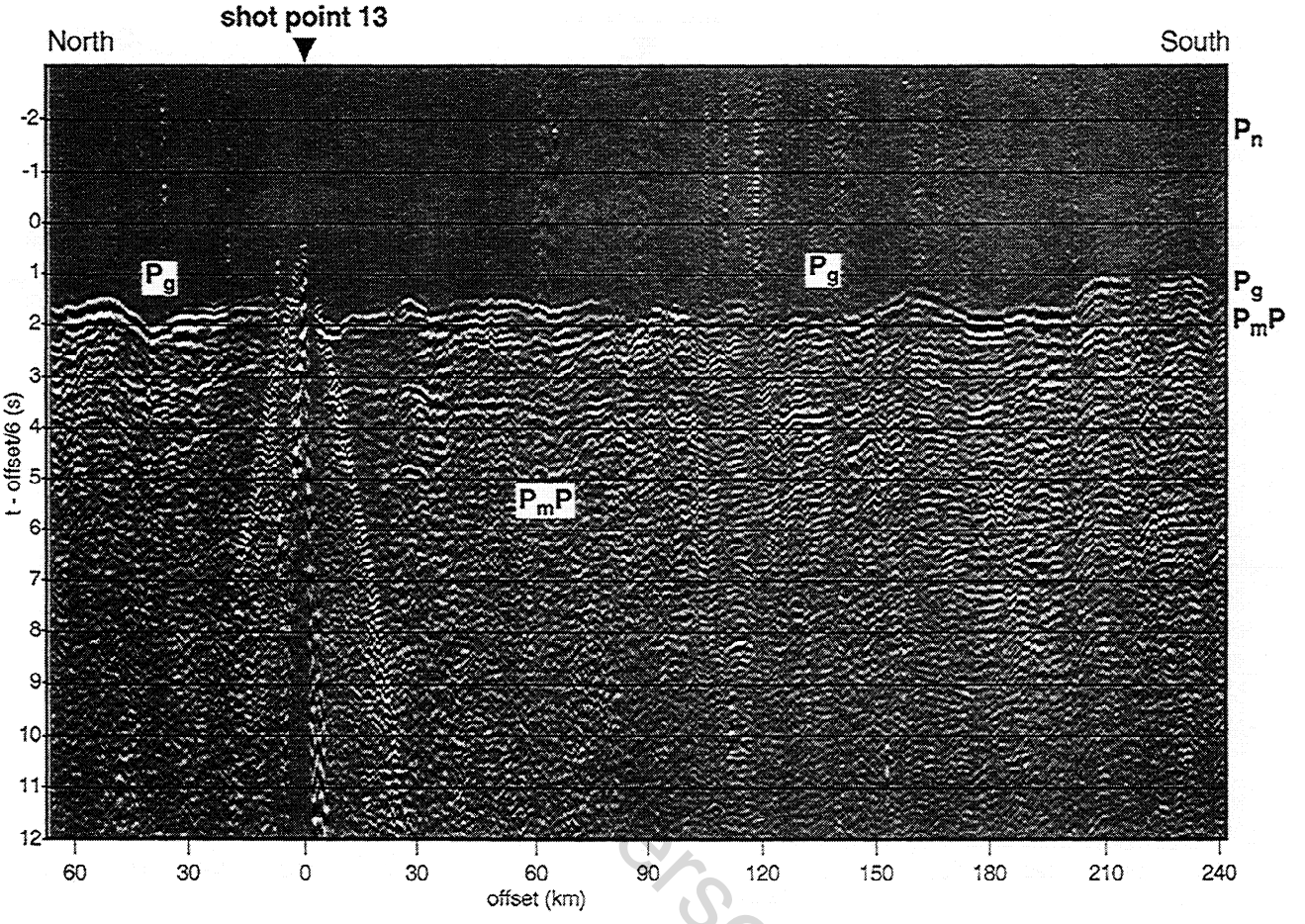

Figure 3d. SSCD gather from shot point 13 displayed with travel time reduced at 6 km/s. Shot point location is indicated by inverted triangle. Shot point 13 is coincident with shot point 43.

phase with a phase-velocity of about 6 km/s even at the largest offsets (Figures 3a, 3d, and 3f) where postcritical $P_m P$ asymptotically converges with P_g. This suggests that velocities stay more or less constant throughout the crust or may even decrease over some interval. The sensitivity of the different arrivals to a mid or lower crustal low-velocity zone is shown in Figure 6 by comparing the travel time fit between our velocity model (Figure 6a) and one that enforces a nonnegative velocity gradient throughout the crust (Figure 6b). Figure 6 displays the shots recorded in the SSCD west-east line, which traverses the Sierra Nevada and shows therefore the strongest effect. The misfits in precritical $P_m P$ and P_n (not shown) can be accommodated in a positive gradient model due to the additional free parameters of Moho depth and mantle velocity as given by *Ruppert et al.* [1998]. In contrast, the misfits at far offsets in P_g can only be reduced in a near-zero gradient model; these misfits are most clearly seen on the NPE shot and the eastern branches of shots 2 and 3.

3. Profiles Through the 3-D Velocity Model

Plate 1 shows seven crustal cross sections through the 3-D velocity model (see Figure 2 for locations) where it is well constrained, overlaid with the location of the Moho and for comparison the Moho from *Mooney and Weaver* [1989], which is a contour map based on older, separate determinations of crustal thickness by multiple authors. The first two profiles follow the two SSCD receiver lines (Plates 1a and 1b). The west-east profile shows that the crust thickens from the Coast Ranges (25 km) to the eastern edge of the Great Valley (40 km), which marks the center of the western Sierra crustal root [*Fliedner et al.*, 1996], and then thins again toward the Basin and Range to just under 30 km (see also contour map of $P_m P$ reflector in Plate 2). Under the westward deepening sediments of the San Joaquin (southern Great) Valley, a high-velocity body stands out at 12–15 km depth. Following *Godfrey et al.* [1997] and *Godfrey and Klemperer* [1998], we interpret this body as Great Valley Ophiolite. It is probably continuous with the Coast Range Ophiolite, which crops out intermittently along the Coast Range thrust system but does not have a clear velocity signature due to mixing with low-velocity Franciscan material [*Godfrey et al.*, 1997; *Godfrey and Klemperer*, 1998]. Almost the entire rest of the crust under the Great Valley Ophiolite and in the Sierra Nevada has unusually low seismic velocities (about 6 km/s). It is unclear whether this near-homogeneity in velocity reflects a homogeneity in

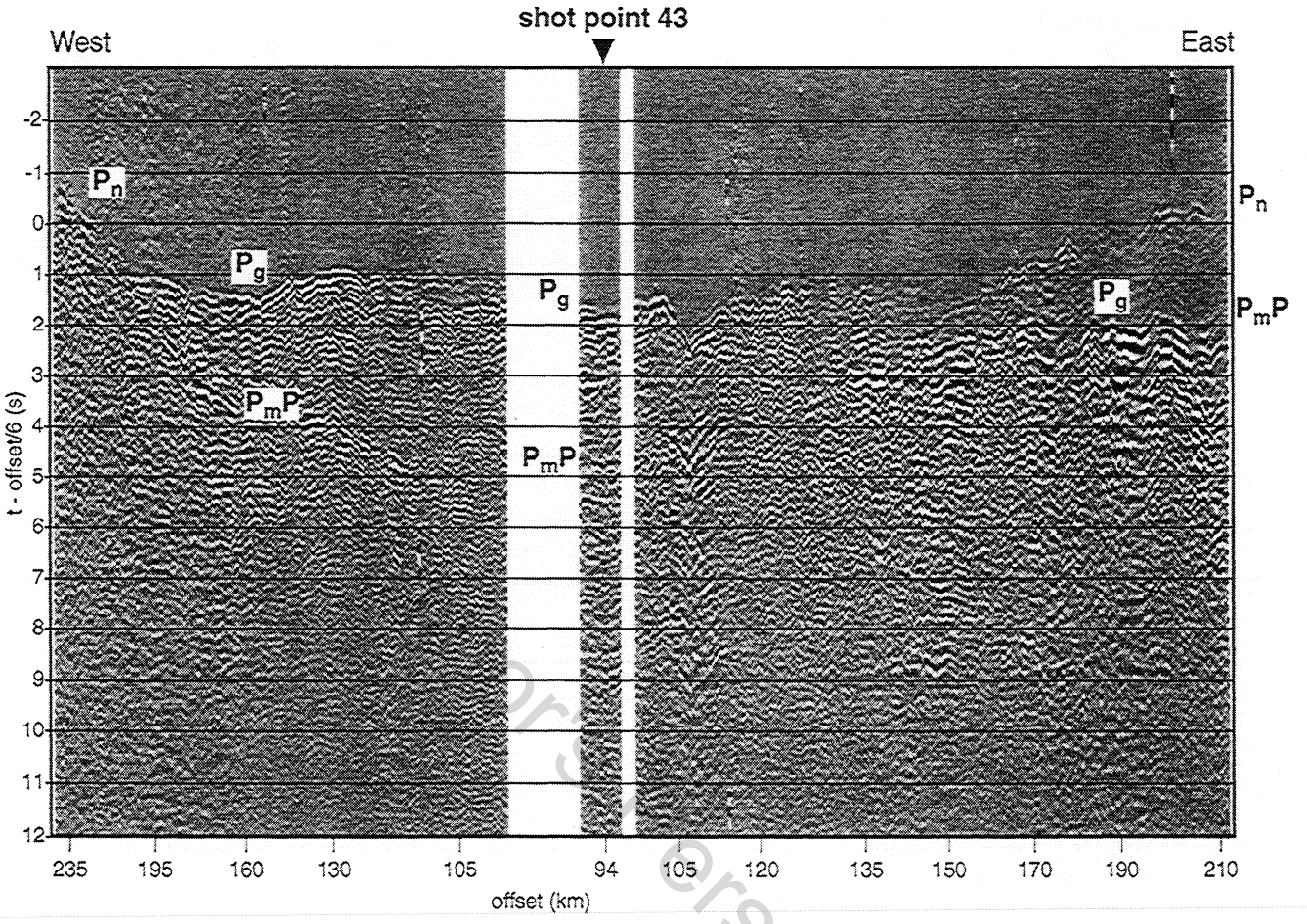

Figure 3e. Same as Figure 3d, except for shot point 43. The inverted triangle marks the projection of the shot point location into the displayed receiver line. Gather is displayed with constant trace spacing (non-linear offset scale).

composition. A tongue of slightly higher velocities near the eastern edge of the San Joaquin Valley (at 125 km on P1, Plate 1a) reaching down to a depth of 25 km could indicate a buried tectonic boundary between the Franciscan assemblage and the Sierra Nevada arc (W. Hamilton, personal communication, 1996). It seems to us, however, more plausible to regard it as a feature within material of Sierran affinity, perhaps a transition from the main Cretaceous batholith to Jurassic, pre-Nevadan arc crust. In any case, the strong contrast between high and low velocities is smeared out in the tomographic inversion (Figure 5). A more detailed interpretation of domains within the low-velocity area must therefore depend on additional geological or geophysical evidence. It is clear, however, that the high velocities under the Great Valley sediments do not continue all the way to the Moho (Figure 6).

Owens Valley (at 230 km on P1, Plate 1a) separates the low-velocity Sierra Nevada from the on-average higher velocity Basin and Range crust near the intersection with the north-south profile (P2, Plate 1b). Except for a 40–70 km wide block under the Panamint Range with velocities under 6 km/s down to a depth of about 18 km, crustal velocities below 5 km depth increase downward from 6.0 to 6.8 km/s (up to 7.0 km/s near the Garlock Fault; Plate 1b). In general, the Basin and Range crust can be divided into an upper crust with a velocity of about 6.0 km/s and a lower crust with a velocity of about 6.4 km/s, separated by a discontinuity at about 17 km depth. Ray tracing of intracrustal phases [*Duran*, 1997] puts the boundary between low upper crustal velocities and higher lower crustal velocities as shallow as 11 km beneath Death Valley and 13 km at the eastern end of the profile.

Velocities of less than 7.6 km/s just below the Basin and Range Moho probably indicate magmatic underplating of the crust. There is no consensus whether to treat this thin layer (up to 5 km) as lowermost crust or uppermost mantle. *Catchings and Mooney* [1991] argue for a 7.4 km/s lower crustal layer and against older studies that identified this layer with the uppermost mantle [see *Catchings and Mooney*, 1991, and references therein] on the grounds that (1) there is a deeper 8.0 km/s layer and (2) the top of the 7.4 km/s layer does not correspond to the Moho as identified by near-vertical reflections [*Klemperer et al.*, 1986]. To be consistent within our study, but in contrast to *Catchings and Mooney* [1991], we place this layer below the Moho as defined by the onset of the wide-angle P_mP reflection. This is not the only place where we find

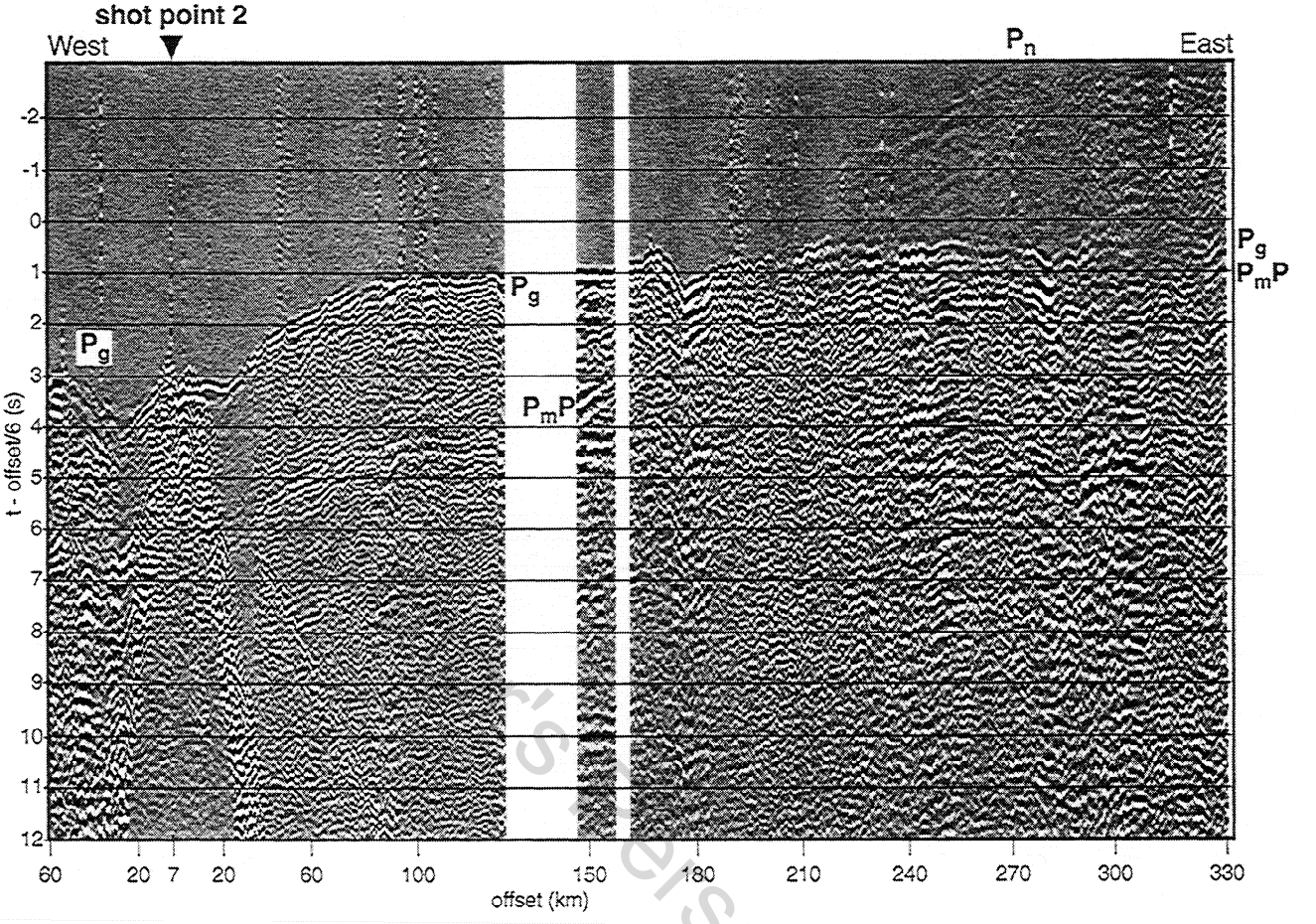

Figure 3f. SSCD gather from shot point 2 displayed with travel time reduced at 6 km/s. The inverted triangle marks the projection of the slightly off-line shot point location into the displayed receiver line.

(in common with previous authors [*Savage et al.*, 1994; *Jones et al.*, 1994]) velocities well below the definition of P_n ($\geq$7.6 km/s), but located beneath the P_mP reflector. We use P_mP as primary criterion for locating the Moho because we have a better distribution of P_mP reflection points than of P_n measurements and it marks almost everywhere the major velocity discontinuity between typical crustal velocities and (usually low) upper mantle velocities. This definition has problems of its own (see below), but is in our judgment the simplest and most consistent. A different question is the geological meaning of a 7.x km/s layer (terminology from *Savage et al.* [1994], and *Jones et al.* [1994]). We return to this problem in the final section.

The two profiles in Plates 1c and 1d are joined at SSCD shot point 19 at the southern end of our model. Lack of short-offset rays from the NPE recording at Nevada Test Site (NTS) prevents us from resolving details of the upper crust in the NE half of the Basin and Range profile (P3, Plate 1c), but it seems to have generally lower velocities than the SW half (6.0 km/s versus 6.2–6.4 km/s). Velocities in the lower crust increase from 6.0 km/s to a maximum of 7.0 km/s (the velocities above 6.6 km/s near the Moho cannot be considered well resolved).

The central and southern Sierra Nevada (Plate 1d, bounded by the Garlock Fault in the south) in contrast reaches velocities of at most 6.4 km/s in the lower crust. On this profile, we also see the most dramatic disagreement of our results with some of the older data: *Mooney and Weaver* [1989] overestimated the thickness of the Sierran crust by roughly 10 km with respect to our model. This difference is partially a matter of semantics as explained above. The difference decreases significantly when we base the comparison on velocities alone. The conventional definition of the refraction Moho (in absence of a clear discontinuity between crustal and mantle velocities) is the 7.6 km/s velocity contour. On the central Sierra profile 4, velocities between the P_mP reflector and the Moho of *Mooney and Weaver* [1989] are about 7.6 km/s. Material with such seismic velocities cannot easily be attributed to either crust or mantle but should be considered a mixture of both. If one takes into account about 10% error in the estimate of absolute Moho depth by either method, we are then left with only one unequivocal area of disagreement: where profiles 1 and 4 intersect. We find there a mantle high with normal mantle velocities, whereas *Mooney and Weaver* [1989] place there the deepest part of a Sierran crustal root. The again quite different interpre-

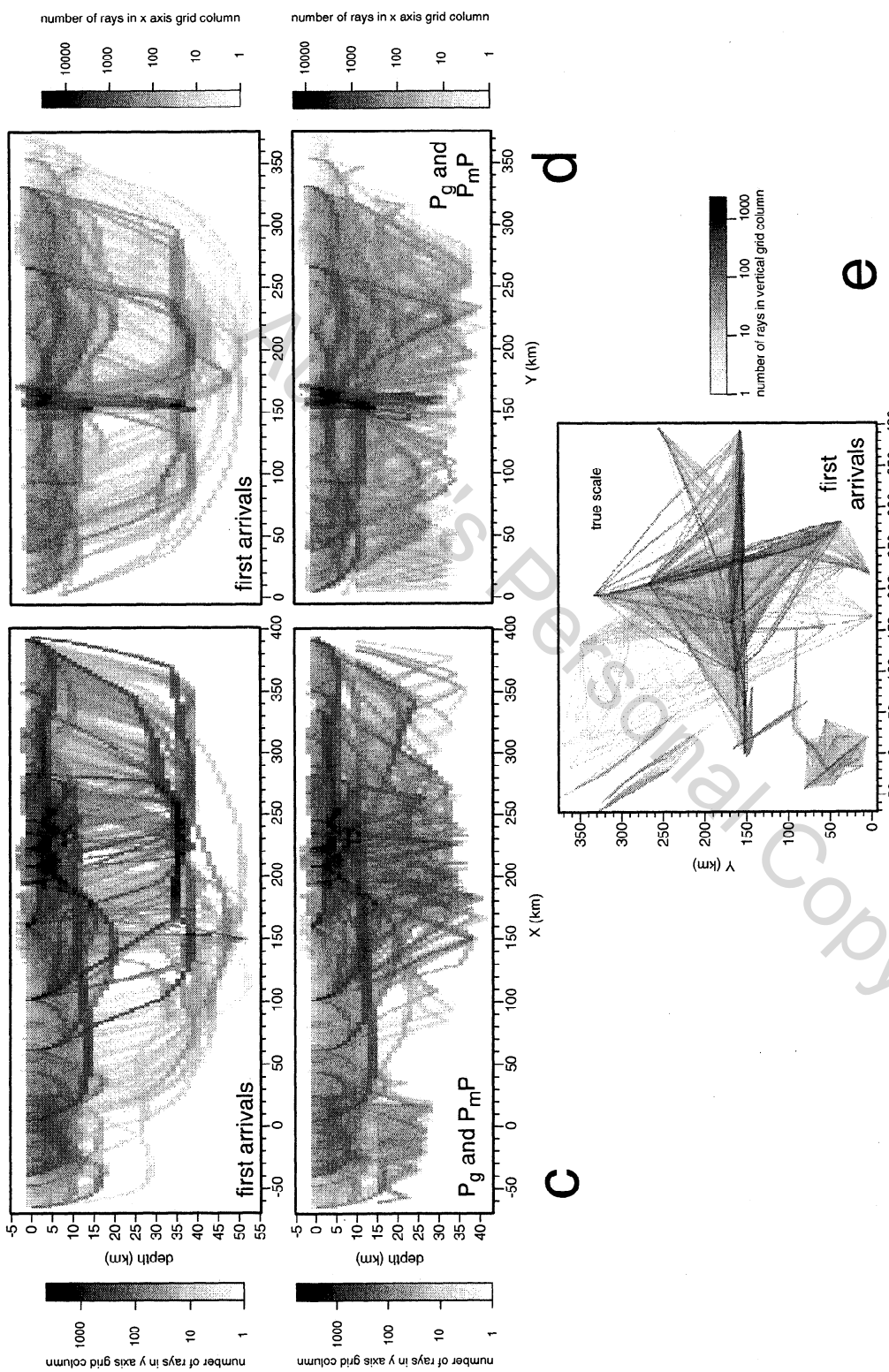

Figure 4. Ray coverage of the finite difference velocity inversion. (a) and (b) First arrivals, (c) and (d) primary and secondary P_g and P_mP, and (e) map view of first arrivals. In each panel the ray counts per cell of the 3-D volume (cell size 1.25×1.25 km) are summed along the axis perpendicular to the page: in Figures 4a and 4c along the Y axis (i.e., a view through the southern X-Z side of the ray cube,) in Figure 4b and 4d along the X axis (i.e., a view through the eastern Y-Z side of the ray cube,) and in Figure 4e along the depth axis (i.e., a bird's eye view through the ray cube). There is a 10:3 vertical exaggeration in Figures 4a–2d.

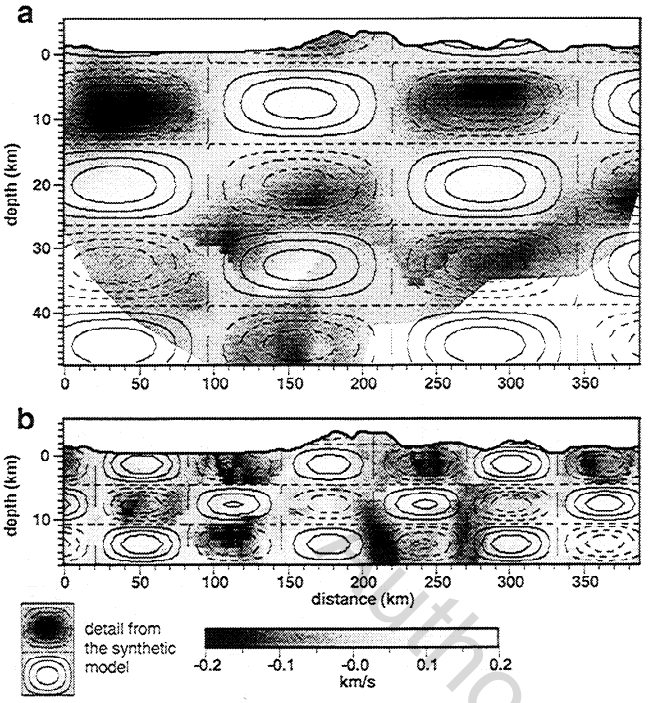

Figure 5. Checkerboard test of model resolution for a cross section along profile P1 (see Figure 2 and Plate 1a). Sinusoidal velocity perturbations of ±0.2 km/s (detail shown below the cross sections) and two different wavelengths are superimposed on a smoothed version of the final P wave velocity model. The reconstruction started with the unperturbed final velocity model and inverted the travel times calculated from the synthetic model as observations. Displayed are the difference between the starting model and the synthetic (i.e., correct) model (contour lines) in comparison with the difference between the starting model and the inversion result (i.e., our best estimate of the synthetic model given the distribution of available data; grayscale). "Success" would be alternating dark and light bull's-eyes as in the detail from the synthetic model, below left. Contour lines are 0.0 (rectangular grid of nodal planes), 0.05, 0.1, and 0.15 km/s (positive solid, negative dashed) deviation of the synthetic model from the starting model.

tation of *Ruppert et al.* [1998] does not resolve that discrepancy, but offers one possible solution: a laminated Moho, that is, a mixture of crustal and mantle material over a depth range of several kilometers. Another possibility, explored further below, is mantle anisotropy: seismic energy that travels along the spine of the Sierra Nevada encounters markedly lowered P_n velocities than that traveling across it. If so, longitudinal profiles would give rise to a crustal root interpretation [*Eaton*, 1966], whereas transverse profiles would yield a rootless interpretation [*Carder*, 1973]. Our isotropic analysis that incorporates sparse arrivals from many azimuths therefore results in a heterogeneous upper mantle with the best trade-off between the two extremes for the data. *Ruppert et al.* [1998] escapes the Eaton-Carder discrepancy because their 2-D interpretations of the west-east and north-south profiles are forcibly reconciled at their intersection and agree within errors both with *Mooney and Weaver* [1989] and with this study.

The last three sections in Plate 1 trace some of the older seismic profiles to the west of the Sierra Nevada. The Great Valley profile (Plate 1e) follows the axis of the San Joaquin Valley. The crust generally thickens from north to south from 20 to 30 km. The high velocities of the Great Valley Ophiolite [*Godfrey and Klemperer*, 1998] can be traced almost continuously along the entire section southward up to the White Wolf Fault, which separates the Great Valley from the southern bend of the Sierra Nevada batholith. Although poorly constrained, our results suggest a velocity decrease below the Great Valley Ophiolite corresponding to older continental crust below the obducted ophiolite [*Godfrey and Klemperer*, 1998]. The Great Valley Ophiolite also shows up as a 10 km thick west dipping body in the profile from the Pacific coast to the eastern edge of the Sierra Nevada (Plate 1f). This is the only area where our seismic data cross the San Andreas Fault. At shallow depth the San Andreas Fault appears as a steep boundary between the low-velocity Franciscan assemblage on the eastern side (Temblor Range of the Coast Ranges) and higher velocity Sierran granitoids in the Salinian block. This velocity contrast vanishes with depth (see also the discussion of the Franciscan/Sierran boundary on profile 1 above). Upper crustal velocities decrease again to the west of the Salinian block in the Sur-Obispo terrane of the western Coast Ranges. A

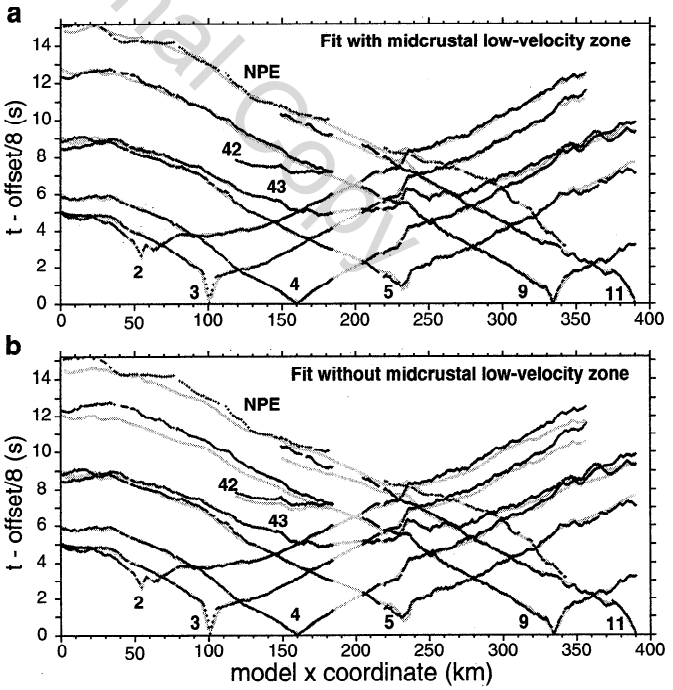

Figure 6. Comparison travel time fit of P_g phase with (a) and without (b) midcrustal low-velocity zone for shots recorded in the SSCD west-east line. Black crosses are travel time picks, gray solid lines the modeled travel times. Traveltimes are reduced at 8 km/s.

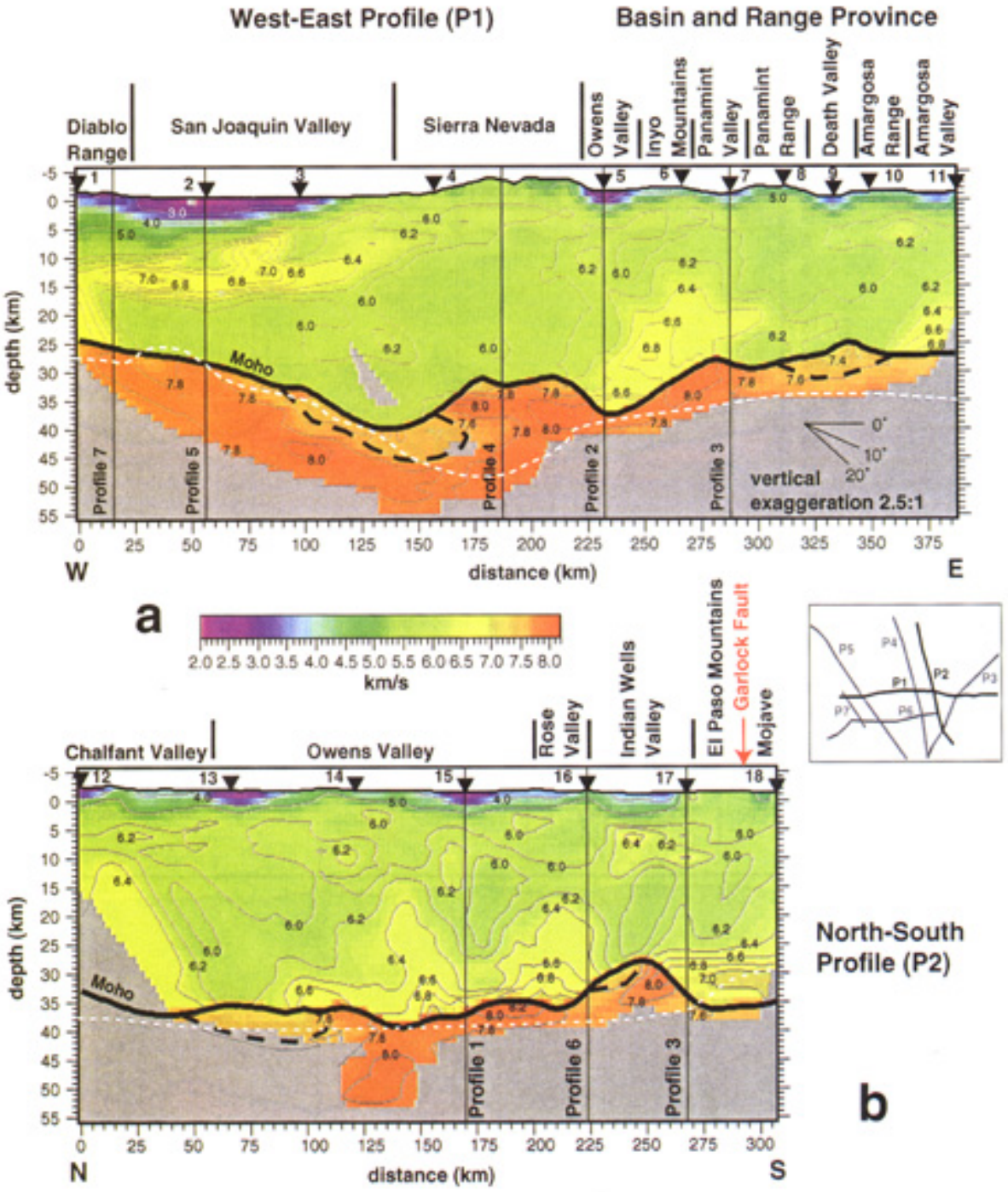

Plate 1. Cross-sections through the 3-D velocity model along profiles (a) P1, (b) P2, (c) P3, (d) P4, (e) P5, (f) P6, and (g) P7 in Figure 2 (see also inset maps). The shaded and contoured areas are constrained in the inversion with nearby rays. Locations of intersecting profiles are marked by vertical lines, inverted triangles mark the locations of shot points (SSCD labeled), and stars mark earthquake hypocenters. Dashed squares in Plate 1d mask unreliable velocities that are solely controlled by direct rays from the earthquake hypocenters below and therefore sensitive to errors in hypocentral depth determination. The thick black line marks the Moho as determined by the P_mP reflector inversion. The white dashed line marks the Moho of *Mooney and Weaver* [1989].

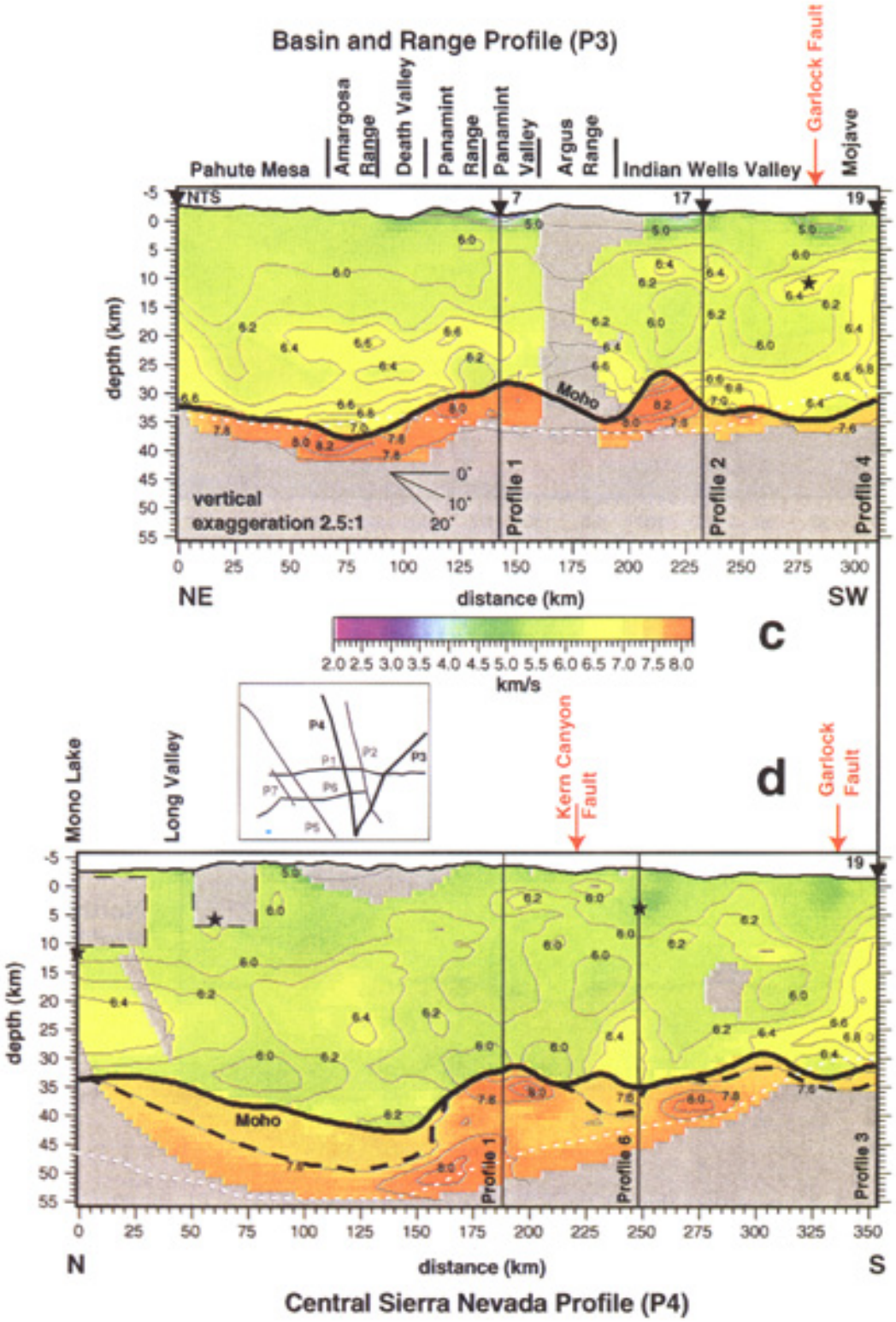

Plate 1. (continued)

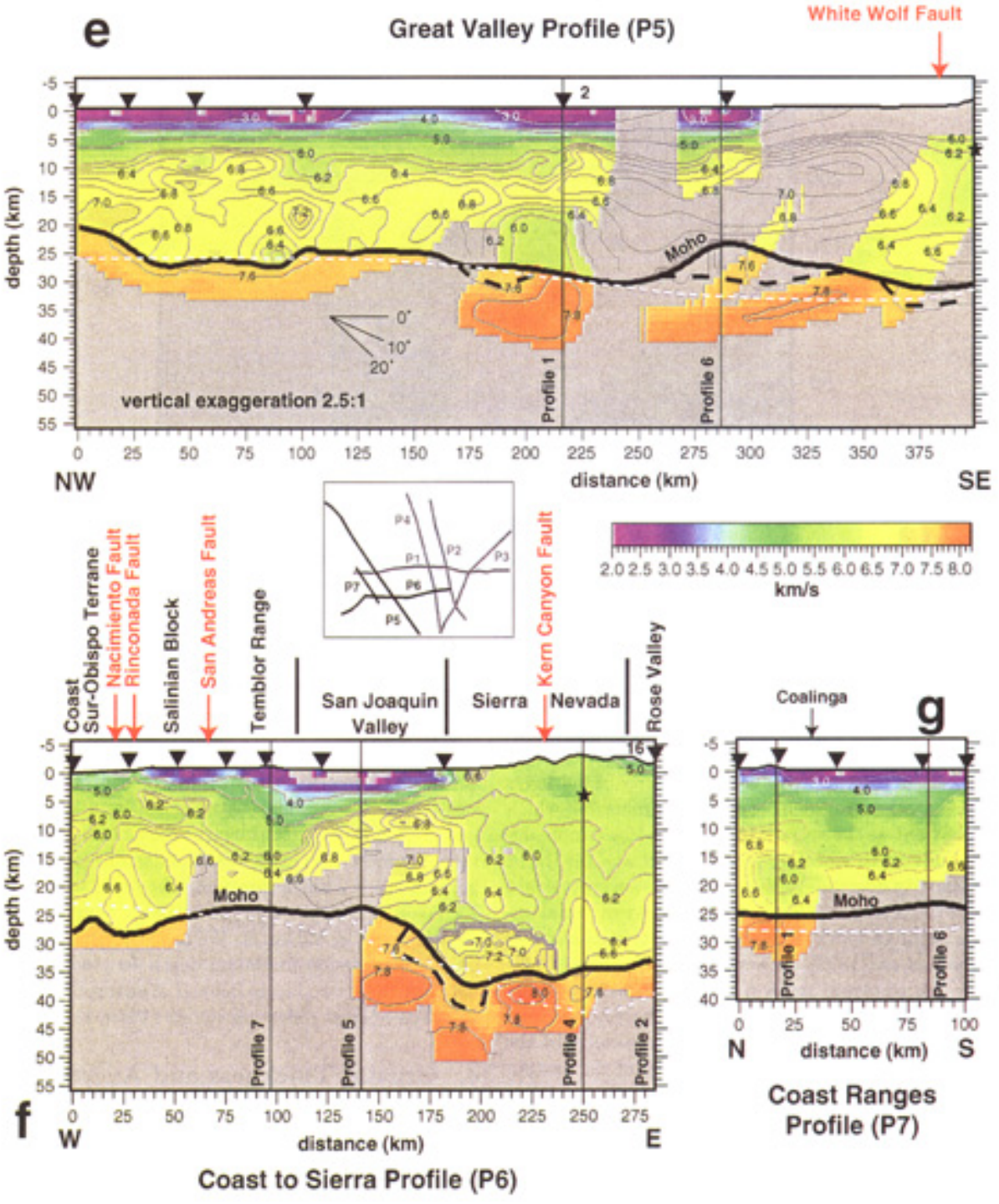

Plate 1. (continued)

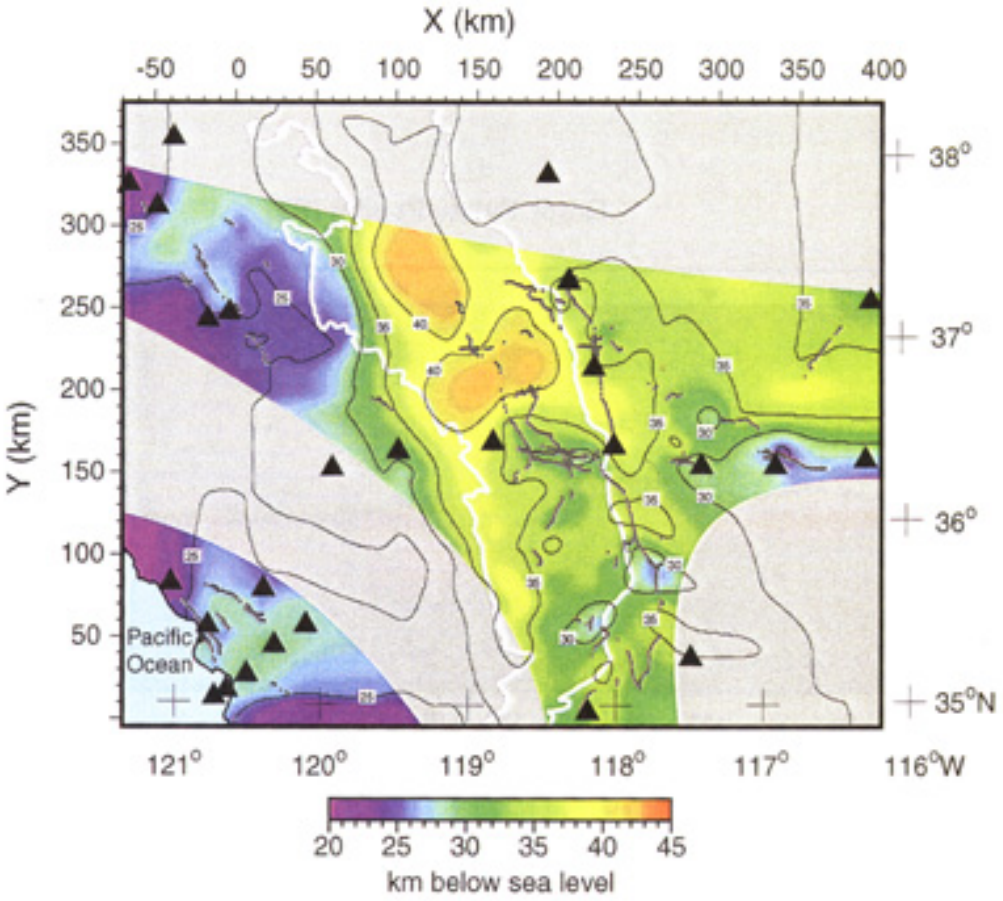

Plate 2. Map of depth to the P_mP reflector. Areas not constrained with nearby reflection points are masked. The Sierra Nevada batholith is outlined in white. Locations of points with P_mP picks are marked with triangles, and P_mP reflection points are marked with gray dots. Thin black lines are Moho depth contours; contour interval is 5 km.

small body at 12 km depth with a velocity of 6.4 km/s could be another fragment of ophiolitic material, which also crops out at the surface in this area (for a more detailed study of this profile, see *Howie et al.* [1993]). A slight velocity decrease in the lower Salinian crust could indicate the presence of Franciscan velocity material under the Salinian block, a possibility that was discussed by *Howie et al.* [1993]. Lower crustal velocities, as far as they are resolved, reach 6.7 km/s, indicating more mafic material either of ophiolitic (subcreted oceanic crust) or lower arc crust origin. The continuity of the ophiolitic material under the Franciscan of the eastern Coast Ranges cannot be determined with the available data (Plate 1g): this short Coast Ranges profile, which links the two west-east running profiles 1 (Plate 1a) and 6 (Plate 1f) through the area of the 1983 Coalinga earthquake [*Wentworth and Zoback*, 1990], shows a velocity increase to only 6.4 km/s except at its northern end where it clearly cuts the Great Valley (or Coast Range) Ophiolite at 15 km depth. Lacking P_mP reflection data, the lower crustal structure between the San Joaquin Valley and the Salinian block remains unresolved.

On the Coast-to-Sierra profile (Plate 1f) under the western Sierra Nevada (between 160 and 225 km), we lack P_mP data to determine the depth of the Moho, but the refraction data of the earthquake data set require a layer of 7.0–7.2 km/s (probably the same as the crustal 7.x layer of *Savage et al.* [1994]) above normal mantle velocities of 7.8–8.0 km/s. We have therefore forced the interface inversion for Moho depth to place the Moho between these two layers instead of extrapolating freely from the nearest reflection points (Plate 2).

4. Crustal Thickness and Average Velocities

The map of Moho depth in Plate 2 is an updated and extended version of the map of *Fliedner et al.* [1996]. It incorporates picks from the Great Valley and San Luis Obispo data sets and the inversion was allowed to produce a somewhat rougher Moho topography to allow a better fit with the travel time data without abandoning the underlying concept of the Moho as a simple reflector. In the final iteration of our inversion we applied horizontal smoothing across a length

scale of 25 km. The inclusion of the earthquake data in the mantle velocity inversion (and to a lesser degree the lowered estimate of lower crustal velocities from secondary P_g) requires a significant reduction (up to 5 km) in Moho depth in the area of shot points 4 and 5 (Plate 1a) compared with the interpretations of *Fliedner et al.* [1996] and *Ruppert et al.* [1998], creating a local mantle bulge with velocities of 7.8–8.0 km/s (profile 1, 170 to 220 km). The SSCD data alone did not require this surprising feature, but the reverberatory nature of the P_mP arrival led *Ruppert et al.* [1998] to infer a laminated Moho (interlayering of material with mantle and crustal velocities) on the basis of synthetic seismogram modeling. Although our interpretation satisfies the travel time constraints of all the data better than *Fliedner et al.* [1996] and *Ruppert et al.* [1998], the introduction of a laminated layer that separates the base of the crust from the top of the mantle allows an overall simpler shape of the Moho and may therefore be the preferable interpretation.

Crustal thickness increases from less than 25 km at the coast to 35–42 km in the western Sierra Nevada and decreases to 30–35 km in the Basin and Range. There seems to be a systematic thinning of the crust from north to south in the Basin and Range reflecting both the decrease in elevation [*Saltus and Thompson,* 1995] and the increase in Bouguer gravity between the northern Basin and Range (Great Basin) and the southern Basin and Range (Mojave-Sonoran Desert).

The major tectonic provinces are also reflected in the average crustal velocities, calculated as a vertical average between the 5 km/s contour (in order to exclude sedimentary basins) and the Moho (Figure 7). Both the Sierra Nevada batholith and the Basin and Range show crustal averages (6.0 to 6.2 km/s) well below the worldwide continental average of 6.45 km/s [*Christensen and Mooney,* 1995]. These low average crustal velocities have important implications for crustal composition, which will be discussed later in this paper. Similar values are found for the Franciscan Coast Ranges and the western side of the Great Valley (at $X = 50$ km) where low-velocity Franciscan assemblage overlies (and underlies?) a very thin Great Valley Ophiolite (Plate 1a, westernmost 50 km of the profile). The rest of the Great Valley is closer to the continental average (6.3–6.6 km/s). The northward increase in velocity is probably due to an increase in thickness of the Great Valley Ophiolite.

The highest average values are observed at the northwestern edge of the Sierra Nevada batholith, at the southern end of the Foothills metamorphic belt and close to a large outcrop of ultramafic and metavolcanic rocks near Fresno ($X = 80$ km, $Y = 220$ km). Considering that velocities here are mainly determined by the sparse earthquake data, this correlation could be fortuitous. *Miller and Mooney* [1994] find similar values for average velocity (6.6 km/s) and crustal thickness (32 km).

5. Velocity-Depth Functions of the Sierra Nevada

The velocity structure of the batholith seems to be very uniform throughout the crust with a velocity that deviates not more than 0.2 km/s from 6.0 km/s (we ignore for the sake of simplicity the upper 5 km of the crust). As discussed above, this interpretation depends on the appearance of the long-offset P_g arrival, which is not compatible even with the low positive velocity gradient in the Sierran lower crust that is allowed by the first-arrival travel times [*Ruppert et al.,* 1998]. We investigate the implications of this unusually low crustal velocity gradient for the composition of the Sierra Nevada by comparing average velocity-depth functions of the Sierra Nevada from our model and that of *Ruppert et al.* [1998] (Figure 8) with velocities measured in the laboratory on two samples of tonalite from the central Sierra Nevada (Table 1 and Figure 9).

Our samples (see Table 2 for chemistry and mineralogy) were collected from fresh road cuts at locations shown in Figure 2. Acoustic velocities of the samples were measured at room temperature and hydrostatic confining pressures to 1000 MPa (equivalent to about 35 km depth) using the pulse transmission technique described by *Christensen* [1985]. Bulk densities were obtained from the weights and dimensions of the cores used for the velocity measurements.

The acoustic velocities were corrected for temperature assuming an average crustal geothermal gradi-

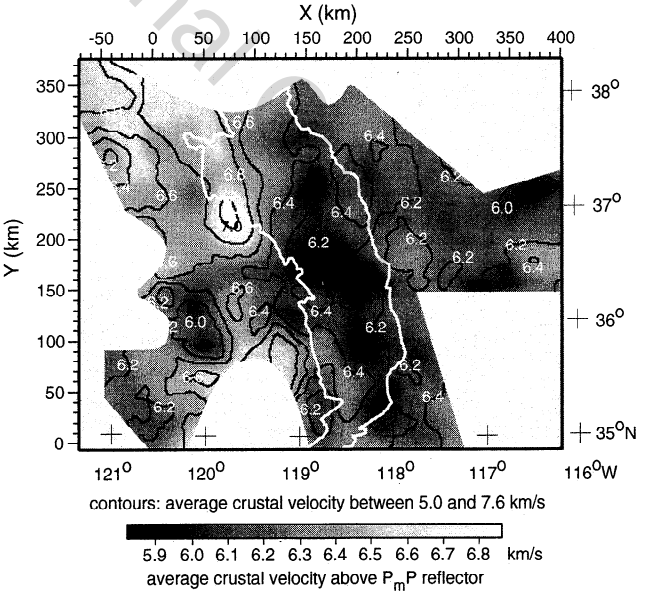

Figure 7. Map of average crustal velocities. Velocities are smoothed averages calculated from the 3-D velocity model in the vertical columns between the 5 km/s contour and the P_mP reflector (grayscale map) or the 7.6 km/s contour (contour map; contour interval 0.2 km/s). The mask outlines roughly the area covered by first arrivals (see Figure 4e). The Sierra Nevada batholith is outlined in white.

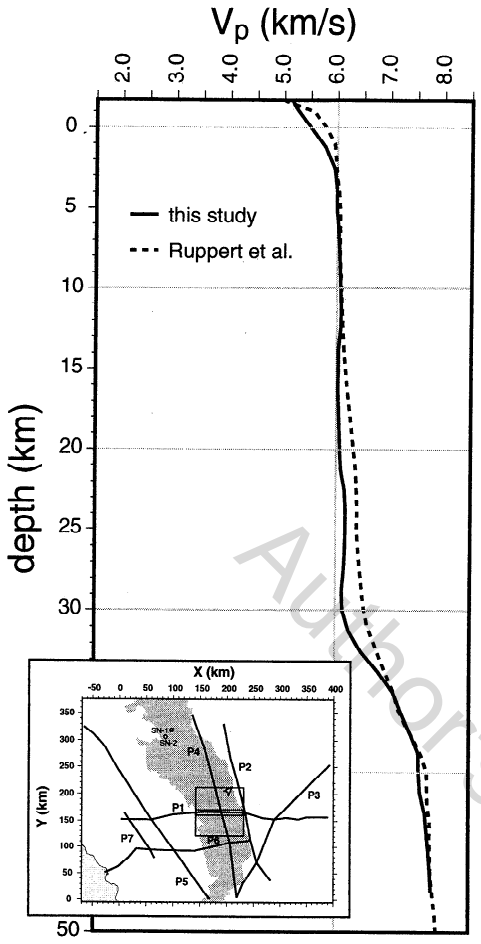

Figure 8. Averaged velocity-depth functions of the Sierra Nevada batholith, extracted from the 3-D velocity model (square outline on inset map) and the 2-D model of *Ruppert et al.* [1998] (rectangular outline around P1 on inset map). Inset map shows location and averaging areas of the velocity functions and locations of tonalitic samples (Figure 9); the Sierra Nevada batholith is shaded in dark gray, profiles of Plate 1 are marked in black.

ent [*Blackwell,* 1971] and a temperature derivative of -0.39×10^{-3} km/s/°C. The densities of the tonalites in Table 1 (2740 kg/m^3) are slightly higher than the average density of 2690 kg/m^3 for Sierra Nevada granodiorites measured by *Oliver et al.* [1993] for about 6000 samples collected from surface exposures throughout the batholith (although our densities agree with *Oliver et al.* [1993] measurements in the western portion of the batholith). For the comparison of average field and laboratory velocity-depth functions, we have lowered our velocities by 0.12 km/s using the linear velocity-density relationship of *Christensen and Mooney* [1995] (Figure 9). This adjusts our tonalite velocities to those of granodiorite with the average granodiorite density determined by *Oliver et al.* [1993].

In the upper 12 km the agreement between field and laboratory measurements is very good, indicating that the granitoids extend to at least this depth. The midcrustal region extending from 12 to 22 km has 0.07 km/s lower velocities than the laboratory measurements. Lower crustal velocities match the laboratory values. However, if this region is granitoid in composition, the batholith rocks have likely recrystallized to granulite facies assemblages, the equilibrium facies under lower crustal conditions. A felsic granulite under these conditions (25 km depth, average heat flow) is expected to have a higher than observed P wave velocity (6.327±0.131 km/s; *Christensen and Mooney* [1995]).

The low-velocity zone in the middle crust could be explained by lowering velocities in granitoid rocks by (1) a lower average density of 2660 kg/m^3. This would produce a mechanically unstable crustal column and requires more radiogenic granite in the batholith than is compatible with the low surface heat flow [*Lachenbruch,* 1968]. The low-velocity zone could also be explained by (2) increased porosity. In igneous rocks where porosity consists primarily of microcracks with high aspect ratios, 1% porosity lowers V_p by about 0.2 km/s at 100 MPa confining pressure [*Christensen,* 1989]. A differential pore pressure of 20 MPa would produce a 0.05–0.1 km/s decrease in V_p at midcrustal confining pressures (Stephenson County Granite given by *Christensen* [1989]). The velocity decrease is largest when the pore pressure approaches the confining pressure.

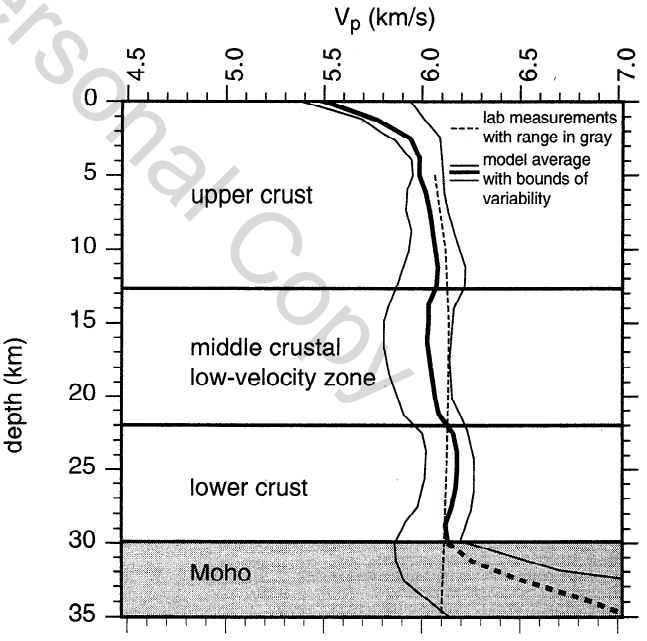

Figure 9. Comparison of velocity-depth function from the 3-D velocity model (Figure 8) and corrected (see main text for details) laboratory measurements on Sierra Nevada tonalite samples (Table 1). The shaded area around the average tonalite values (thin dashed line) shows the range of values measured on the two samples. The thin solid outline around the average velocity-depth function from the 3-D velocity model shows the variation of velocities within the area over which the average has been calculated. The depth to the Moho varies over the averaging area.

Table 1. Laboratory Measurements on Field Samples of Two Eastern Sierra Nevada Tonalites SN-1 and SN-2

Sample	SN-1A, 2742 kg/m^3		SN-1B, 2734 kg/m^3		SN-1C, 2745 kg/m^3		SN-2A, 2746 kg/m^3		SN-2B, 2727 kg/m^3		SN-2C, 2738 kg/m^3	
Depth, km	V_p, m/s	V_s, m/s	V_p, m/s	V_s, m/s	V_p, m/s	V_s, m/s	V_p, m/s	V_s, m/s	V_p, m/s	V_s, m/s	V_p, m/s	V_s, m/s
5	6267	3595	6243	3584	6217	3617	6206	3665	6147	3593	6221	3620
10	6339	3614	6328	3610	6299	3637	6297	3693	6255	3624	6300	3647
15	6379	3625	6374	3624	6344	3646	6342	3706	6306	3641	6344	3662
20	6406	3633	6405	3633	6375	3651	6370	3714	6340	3652	6374	3672
25	6426	3639	6429	3641	6398	3656	6388	3721	6365	3661	6397	368
30	6441	3644	6447	3647	6415	3660	6403	3727	6385	3669	6414	3686
35	6453	3648	6462	3652	6430	3663	6413	3732	6401	3675	6428	3691

See Figure 2 for locations. Three perpendicular cores A, B, and C were measured at different pressures (here converted to depth) at room temperature, and their densities were measured at atmospheric pressure. Poisson's ratio at 500 MPa (27 km depth): 0.262 ($V_p/V_s = 1.760$) for SN-1 and 0.250 ($V_p/V_s = 1.732$) for SN-2.

Table 2. Chemistry and Mineralogy of Two Eastern Sierra Nevada Tonalites SN-1 and SN-2

Sample	SiO_2, %	Al_2O_3, %	Fe_2O_3, %	MgO, %	CaO, %	Na_2O, %	K_2O, %	TiO_2, %	P_2O_5, %	MnO, %	Cr_2O_3, %	Ba, ppm	Ni, ppm	Sr, ppm	Zr, ppm	Y, ppm	Nb, ppm	Sc, ppm	Total %
SN-1	61.98	17.53	5.81	2.11	5.73	3.75	1.66	0.81	0.22	0.08	0.007	679	29	656	156	<10	10	<10	100.41
SN-2	61.99	17.59	5.73	2.20	5.72	3.72	1.78	0.86	0.21	0.08	0.005	808	<20	651	165	11	<10	<10	100.63

	Biotite	Hornblende	Sphene	Magnetite	Chlorite	Plagioclase	Quartz	K-feldspar
SN-1	17	4	1	1	1	55	13	8
SN-2	15	3	1	1	1	54	15	10

See Figure 2 for locations. Mineralogy in volume percent.

An increase in pore pressure also produces an increase in Poisson's ratio, but this is precluded by results of *Jones and Phinney* [1998] which show no increase in Poisson's ratio for the 12 to 22 km depth range, but only below 24 km depth. The low-velocity zone could be explained by (3) increased temperature. An increase in temperature of 180°C over the assumed average geotherm would bring the laboratory measurements into agreement with the velocity model and would make felsic granulite (0.09 km/s reduction in P wave velocity) rather than unmetamorphosed granitoids compatible with the observed seismic velocities in the lower crust (felsic granulites as defined and measured by *Christensen and Mooney* [1995]). Poisson's ratio is not affected by an increase in temperature. A heat pulse from the mantle that has reached the low-velocity zone as given by *Crough and Thompson* [1977] could be the source for this temperature increase. It would only take 2 to 4 million years for a thermal disturbance to travel from the base of the crust to the top of the low-velocity zone (using the estimate of *Crough and Thompson* [1977]), considerably less than the 10 million years assumed in their uplift model for the Sierra Nevada. The low-velocity zone could be explained by (4) crustal anisotropy. Assuming that the granitoids become gneissic with depth, the low-velocity zone could be the result of waves traveling perpendicular to the prevailing foliation of midcrustal rocks. Since the paths of the rays that determine the low-velocity zone are mainly east-west and mainly horizontal, the foliation would be vertical and parallel to the batholith. Tonalitic gneiss at 15 km depth typically exhibits a P wave anisotropy of 9% in laboratory measurements [*Christensen and Mooney,* 1995], more than enough to account for the 1–2% needed to explain the low-velocity zone. *Ducea and Saleeby* [1996] observed gneissic texture in xenoliths of granodioritic compositions in the eastern Sierra Nevada.

6. Upper Mantle Velocities

Measurements of P_n velocities are sparse and far from uniformly distributed in our data set. They come from the shots at the ends of the two SSCD profiles, the NPE shot at Nevada Test Site and the earthquake data set. The inversion of these data points for an isotropic velocity model results in a highly heterogeneous upper mantle. The very generalized pattern is a southward velocity increase in the Sierra Nevada (Plates 1b and 1d) and (arguably) in the Great Valley (Plate 1e) and a westward increase across the Sierra Nevada into the westernmost Basin and Range province (Plate 1a). The highest velocities (8.0–8.2 km/s) are observed directly beneath the Moho of the southwestern Sierra Nevada and westernmost Basin and Range (Plates 1a–1c). The lowermost velocities of 7.4–7.6 km/s beneath the central Sierra Nevada (Plate 1d) and some parts of the Basin and Range (Plate 1a) could equally well be called lower crust albeit with a bigger velocity contrast with the rest of the crust than with the rest of the upper mantle. A velocity of about 7.8 km/s seems to be regional average. We refrain from actually calculating an average because of the nonuniform ray coverage, both areally and in depth, and the bias toward low, possibly crustal velocities, that our definition of the Moho as the P_mP reflector entails. In the following paragraphs we refer to "P_n velocity" rather than upper mantle velocity when we mean to exclude the velocities below 7.6 km/s.

The pattern of the velocity distribution, however, allows the possibility that at least some of the velocity extremes indicate strong seismic anisotropy rather than a heterogeneous (but isotropic) mantle as we have modeled; almost all the low velocities derive from ray paths along the strike of the Sierra Nevada batholith (especially the earthquake data set), whereas the high velocities derive from ray paths across the Sierra Nevada (which also sample the Basin and Range province). The sparseness of the P_n ray coverage permits a separation of the high and low velocities both horizontally (low under the batholith, high under the Basin and Range) and vertically (high and low directly beneath the Moho, average at greater depths) in our isotropic model. *Sung and Jackson* [1992] report low mantle velocities (7.4–7.7 km/s) under the southernmost Sierra Nevada near White Wolf Fault (see Plate 1e); they also found significant P_n anisotropy of about 3% (0.22±0.08 km/s) with a fast direction N75°±4°W. Anisotropy in the mantle can be produced by aligning the fast axes of olivine grains (aaaxis). Measurements on upper mantle xenoliths from the central Sierra Nevada produce a P wave anisotropy of 6% [*Scott and Christensen,* 1996], which can easily explain the entire range of observed P_n velocities.

Studies from two xenolith localities suggest that the upper mantle is anisotropic beneath the Sierra Nevada batholith. *Peselnick et al.* [1977] report anisotropies of 0.5–0.6 km/s for two peridotite xenoliths collected from a basalt pipe near Big Creek, Fresno County, on the western flank of the central Sierra Nevada. In addition, we have measured olivine petrofabrics for three peridotite xenoliths collected from the Oak Creek region (Figure 2) located on the eastern flank of the Sierra Nevada [*Ducea and Saleeby,* 1996]. The peridotites show weak foliation and average 90% olivine. Using a 5-axis universal stage, 100 grains were selected for orientation from each specimen. Contoured axis orientations with foliations oriented parallel to the page are shown in Figure 10.

The fabric diagrams show that olivine orientation is relatively uniform for the three peridotites. Olivine crystallographic a axes show strong concentrations and lie in the foliation planes. The maxima of the olivine crystallographic b axes tend to fall approximately normal to the foliations. A strong b axes maximum is consistent with an origin by high-temperature plastic flow with slip on olivine (010) (plane perpendicular to b axis)

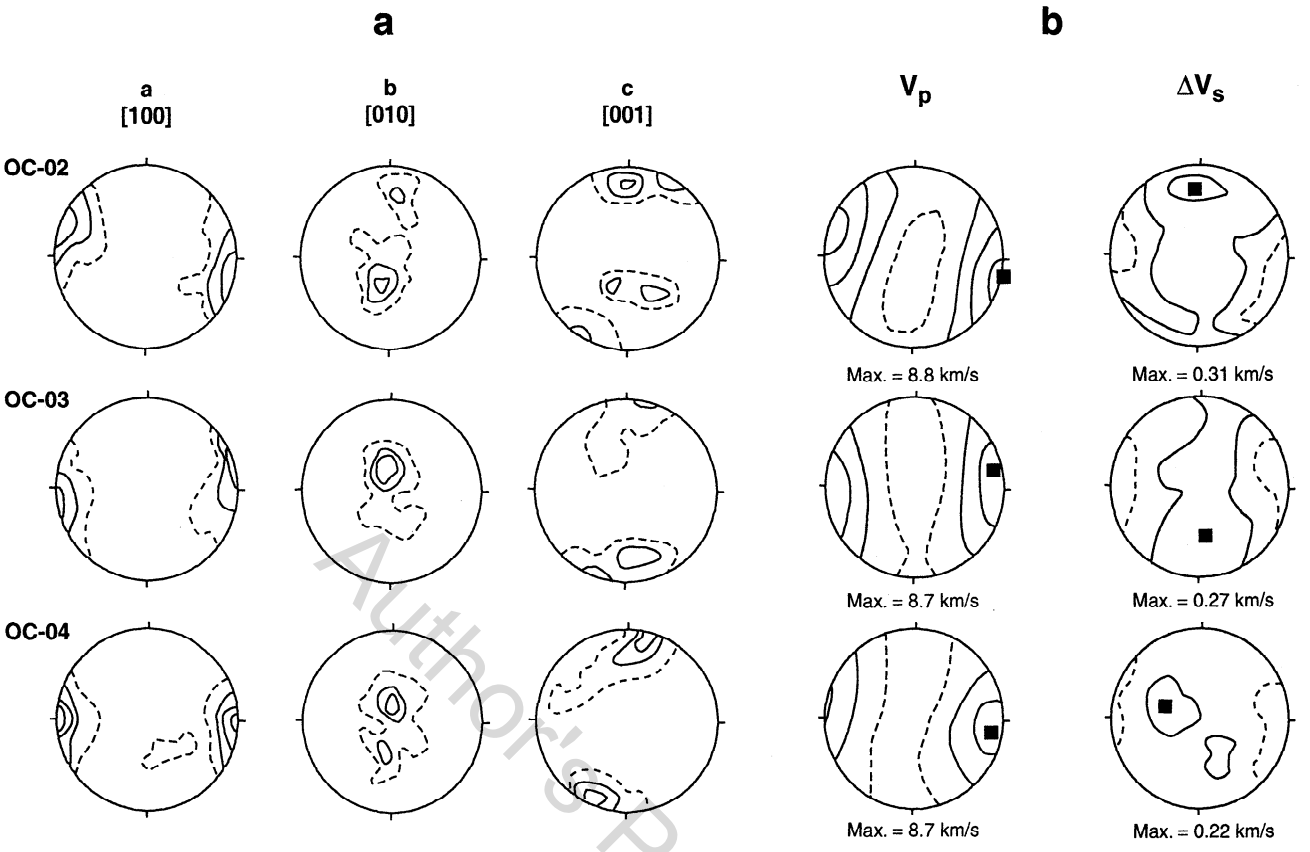

Figure 10. Anisotropy measurements on Oak Creek xenolith samples OC-02, OC-03, and OC-04 (eastern Sierra Nevada). Host rock is a 150,000 year old volcanic pipe [*Ducea and Saleeby,* 1996]. Xenoliths are spinel peridotites; depth estimates based on clinopyroxene barometry are 29 to 34 km. (a) Equal-area, lower hemisphere projections of a, b, and c axes of olivine. Contour interval is 2% per 1% area. Minimum contours (2%) are shown as dashed lines. (b) Compressional velocity anisotropy and shear wave splitting anisotropy. Contour intervals are 0.2 km/s for V_p and 0.1 km/s for ΔV_s. Minimum contours are shown as dashed lines and maximum values correspond to solid squares.

in the [100] (a axis) direction [*Carter and Avé Lallemant,* 1970; *Nicolas et al.,* 1973]. The olivine crystallographic c axes show slightly weaker orientations than the a- and b axes and tend to subparallel foliations.

We have calculated velocity anisotropies of the xenoliths at a confining pressure of 1000 MPa from the fabric diagrams using the computer program of *Crosson and Lin* [1971]. From the single-crystal elastic constants of olivine, their pressure derivatives, and the universal-stage orientation data of each olivine crystal, the program calculates the contribution of each mineral to the rock velocities in specified directions. One compressional wave velocity and two shear wave velocities, with perpendicular polarization directions, are given as output for each specified propagation direction. These velocities were then contoured to show the total anisotropy patterns in three dimensions. In Figure 10, contoured diagrams are given for compressional wave velocity (V_p) and shear wave splitting (ΔV_s). Actual velocities and anisotropies will be lower because of temperature and presence of up to 20% pyroxene (olivine 8.45 km/s and orthopyroxene 7.85 km/s).

Our study cannot constrain to what degree the P_n velocity variations in this region are a result of compositional and thermal variations or of seismic anisotropy in peridotite (eclogite in contrast is largely isotropic [*Christensen and Mooney,* 1995]), but we have shown that the measured anisotropy in the Oak Creek xenoliths, if representative of a regionally developed mantle fabric, is on its own sufficient to explain our seismic observations.

7. Tectonic Implications and Conclusions

A schematic cross section through California is shown in Figure 11. It combines details from the two west-east profiles 1 and 6 (Plates 1a and 1e). To the west of the San Andreas Fault are terranes moving northward with the Pacific plate. To the east of the San Andreas

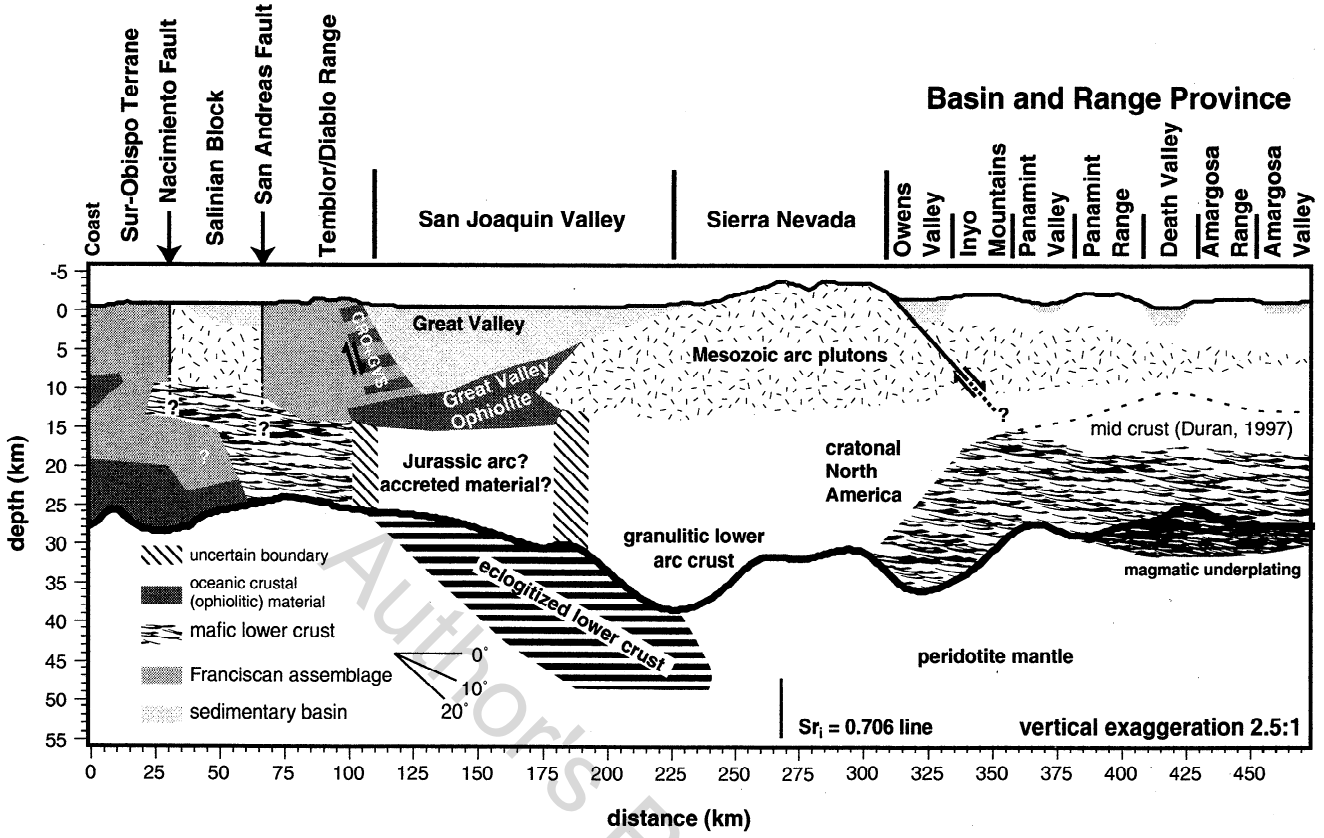

Figure 11. Schematic cross section through south-central California (at roughly 36° latitude) combining the velocity profiles P1 (Plate 1a) and P6 (Plate 1f). Thick black line marks seismic Moho. Location of the line of initial $^{87}Sr/^{86}Sr = 0.706$, thought to be roughly coincident with edge of North American craton, from *Kistler and Peterman* [1978]. CRO+GVS is Coast Range ophiolite and Great Valley sequence [*Godfrey and Klemperer*, 1998]. The extent of faults in the lower crust is uncertain.

Fault are the former subduction zone and arc complex, represented by the Franciscan assemblage and Great Valley Sequence/Great Valley Ophiolite in the forearc, the Sierra Nevada as the former volcanic arc, and the Basin and Range province in the backarc.

There is a relatively clear division between the terranes west of the Great Valley. Crustal velocities generally decrease from west to east. In the Sur-Obispo terrane the high and low velocities are probably due to a mixture of ophiolitic or intruded material (in the middle crust) and remnant oceanic crust (in the lower crust) with low-velocity Franciscan assemblage [*Howie et al.*, 1993]. The Salinian block is believed to be a piece of Sierra Nevada arc transported northward by the San Andreas Fault [*Whidden et al.*, 1998, and references therein; *James*, 1992]. On the east side of the San Andreas Fault, the Franciscan assemblage has lower velocities than the Salinian in the upper 15 km but is indistinguishable from the Salinian below that depth. There is no seismic velocity contrast between the Franciscan and the Great Valley Sequence or Coast Range Ophiolite above the high-velocity body of the Great Valley Ophiolite (*Godfrey and Klemperer* [1998] found the same in the northern Coast Ranges/Great Valley). The lower crust on the west side of the Great Valley is not visible in our data.

Figure 11 shows the Sierra Nevada arc continuing beneath the Great Valley Ophiolite. Since there is no significant difference in velocity between the deep crust of the Franciscan assemblage and the Sierra Nevada, it is not possible to draw the boundary between the two on the basis of the present seismic data. Neither is there a clear seismic expression of the boundary between the Precambrian North American craton and the younger accreted terranes to the west. This boundary is usually thought to coincide with the $Sr_i = 0.706$ line [*Kistler and Peterman*, 1973, 1978] in the Sierra Nevada batholith, which coincides with an isostatic residual gravity gradient [*Jachens and Griscom*, 1985]. This means that, in order to satisfy the seismic velocities, at least in the eastern Sierra Nevada parts of the lower crust consist of continental felsic granulites or metapelites with protoliths that predate the formation of the arc. The only surface-seismic indication of structure within the Sierra Nevada crust is the slight velocity decrease in the midcrust. Although seismic velocities require a felsic composition throughout the crust, the low surface heat flow in the Sierra Nevada, the linear heat

flow-heat production correlation observed by *Lachenbruch* [1968] and surficial density variations [*Saltus and Lachenbruch,* 1991; *Oliver et al.,* 1993] suggest a base of granitoids (with heat-generating radiogenic U, Th, and K) at a depth of about 10 km [*Lachenbruch,* 1968]. The midcrustal low-velocity zone is therefore probably the base of the plutons that characterizes the Sierra Nevada at the surface. In the middle and lower crust, gneisses or felsic granulites (whether older continental material, or radiogenically depleted arc plutons) with a low heat production must prevail. Increased lower crustal temperatures that have not yet affected the low surface heat flow in most parts of the Sierra Nevada would indeed make felsic granulite the composition that matches the observed velocities (see section 5).

In the Mesozoic the arc must have looked very different from the present-day Sierra Nevada crust if it was then a typical continental arc. *Holbrook et al.* [1992] show the crustal column of an average arc to consist of 22 km of upper and middle crust with a bimodal velocity distribution (6.1 and 6.6 km/s) and 16 km of lower crust with a velocity of 6.8–7.0 km/s. The exposed Kohistan arc section in Pakistan [*Miller and Christensen,* 1994] consists of a 15 km thick granodioritic upper crust followed by 3 km of diorite with velocities of 6.0 to 6.9 km/s and a 25 km thick metagabbroic and amphibolitic lower crust with velocities of 7.0 to 7.5 km/s. The modern Sierra Nevada seems to have retained only the upper crustal and midcrustal part of that column (at the low end of the velocity distribution). A high-velocity lower crust is completely absent. This missing lower crust would have had a mafic composition (metagabbro, mafic granulite, or amphibolite) and must have been present during arc formation according to current models of the generation of continental crust [e.g., *Taylor and McLennan,* 1995]. At least for the deepest parts of the arc crust, the problem of the "missing" mafic residue may be partially semantic: *Rapp and Watson* [1995], among others, point out that the residue would be a garnet pyroxenite, an eclogite facies rock. Eclogites have seismic velocities above 7.6 km/s [*Christensen and Mooney,* 1995], placing them in the seismic mantle. Xenoliths of the appropriate composition have been found in the central Sierra Nevada [*Ducea and Saleeby,* 1996, 1998b] (see below). The up to 10 km of sub-7.6 km "mantle" found in the central and western Sierra Nevada must be composed of garnet granulite, pyroxenite, eclogite, or a mixture of such lithologies as the velocities are too low for peridotite unless the upper mantle is partially molten. Partial melt as an explanation for low upper mantle and lower crustal velocities is supported by magnetotelluric evidence for enhanced conductivity in the lower crust and upper mantle of the Great Valley, western Sierra Nevada, and Owens Valley [*Park et al.,* 1996]. Since the thermal conditions in the upper mantle are so uncertain, seismic velocities alone are insufficient to infer its composition. As peridotites in contrast to eclogites can be strongly anisotropic, measuring the regional distribution of sub-Moho anisotropy would make an important contribution to resolving this problem.

In conclusion, we can make a rough estimate how thick the complete Sierra Nevada arc was originally. We assume the same proportions of upper/middle and lower crust as in the average arc of *Holbrook et al.* [1992] applied to the Mesozoic Sierra Nevada although that "average arc" may be biased toward island arcs. The depth of crystallization exposed at the surface at the latitude of our cross section is 8 to 15 km [*Ague and Brimhall,* 1988]. So if we add 10 km of eroded upper crust to the existing 35 km of low-velocity crust we form an original arc upper crust and midcrust of 45 km. This includes, at least in the eastern Sierra Nevada, an unknown amount of preexisting North American continental crust and can therefore be considered an upper bound. Forty five kilometers of original felsic crust imply an original mafic lower crust of about 30 km and a Mesozoic crustal column of 75 km thickness, comparable to the modern Andes [*Zandt et al.,* 1994]. Only about a third of this conjectural lower crust can be accounted for by the up to 10 km thick layer of extremely low sub-Moho velocities found beneath much of the central and western Sierra Nevada that is most likely to represent an eclogite facies lower crust. This layer balances hardly more than the now eroded top of the arc. Furthermore, the higher upper mantle velocities and the presence of peridotite xenoliths suggest that such a subcrustal layer is absent in the eastern Sierra Nevada. The remainder of the original lower arc crust if still present at all is now indistinguishable from the surrounding mantle.

Acknowledgments. This study was supported by National Science Foundation (NSF) Continental Dynamics Program grant EAR-93-16008. The laboratory studies were funded by NSF Continental Dynamics Program grant EAR-93-17522. The petrofabrics were measured by Kim Schram at Purdue University, West Lafayette, Indiana. We thank the reviewers, especially R. Saltus, C. Jones, G. R. Keller, and M. Ducea, and the Associate Editor W. Mooney for their detailed and insightful (even if sometimes tough) comments.

References

Ague, J. J., and G. H. Brimhall, Magmatic arc asymmetry and distribution of anomalous plutonic belts in the batholiths of California: Effects of assimilation, crustal thickness, and depth of crystallization, *Geol. Soc. Am. Bull., 100,* 912–927, 1988.

Blackwell, D. D., The thermal structure of the continental crust, in *The Structure and Physical Properties of the Earth's Crust,* Geophys. Monogr. Ser., vol. 14, edited by J. G. Heacock, pp. 169–184, AGU, Washington, D. C., 1971.

Carder, D. S., Trans-California seismic profile, Death Valley to Monterey Bay, *Bull. Seismol. Soc. Am., 63,* 571–586, 1973.

Carter, N. L., and H. G. Avé Lallemant, High temperature flow of dunite and peridotite, *Geol. Soc. Am. Bull., 81,* 2181–2202, 1970.

Catchings, R. D., and W. D. Mooney, Basin and Range crustal and upper mantle structure, northwest to central Nevada, *J. Geophys. Res., 96*, 6247–6267, 1991.

Christensen, N. I., Measurement of dynamic properties of rock at elevated pressures and temperatures, in *Measurement of Rock Properties at Elevated Pressures and Temperatures,* edited by J. Pincus and E. R. Hoskins, pp. 93–107, Am. Soc. for Test. and Mater., West Conshohocken, Pa., 1985.

Christensen, N. I., Pore pressure, seismic velocities, and crustal structure, in *Geophysical framework of the continental United States,* edited by L. C. Pakiser and W. D. Mooney, *Mem. Geol. Soc. Am., 172,* 783–798, 1989.

Christensen, N. I., and W. D. Mooney, Seismic velocity structure and composition of the continental crust: A global view, *J. Geophys. Res., 100*, 9761–9788, 1995.

Colburn, R. H., and W. D. Mooney, Two-dimensional velocity structure along the synclinal axis of the Great Valley, California, *Bull. Seismol. Soc. Am., 76*, 1305–1322, 1986.

Colburn, R. H., and A. W. Walter, Data report for two seismic-refraction profiles crossing the epicentral region of the 1983 Coalinga, California, earthquakes, *U.S. Geol. Surv. Open File Rep., 84-643,* 57 pp., 1984.

Crosson, R. S., and J. Lin, Voight and Reuss prediction of anisotropic elasticity of dunite, *J. Geophys. Res., 76,* 570–578, 1971.

Crough, S. T., and G. A. Thompson, Upper mantle origin of Sierra Nevada uplift, *Geology, 5,* 396–399, 1977.

Ducea, M. N., and J. B. Saleeby, Buoyancy sources for a large, unrooted mountain range, the Sierra Nevada, California: Evidence from xenolith thermobarometry, *J. Geophys. Res., 101*, 8229–8244, 1996.

Ducea, M. N., and J. B. Saleeby, A case for delamination of the deep batholithic crust beneath the Sierra Nevada, California, *Int. Geol. Rev., 40,* 78–93, 1998a.

Ducea, M. N., and J. B. Saleeby, The age and origin of a thick mafic-ultramafic keel from beneath the Sierra Nevada batholith, *Contrib. Mineral. Petrol., 133,* 169–185, 1998b.

Duran, A. E., A crustal structure study of the Owens Valley-Death Valley region, eastern California, M.S. thesis, Univ. of Texas, El Paso, 1997.

Eaton, J. P., Crustal structure in northern and central California from seismic evidence, in *Geology of Northern California*, Bull. Calif. Div. Mines Geol., *190*, 419–426, 1966.

Fliedner, M. M., Making of continental crust by arc magmatism: Wide-angle seismic and gravity studies in the southern Sierra Nevada of California and the eastern Aleutian Arc, Ph.D. thesis, 166 p., Stanford Univ., Stanford, Calif., 1997.

Fliedner, M. M., S. Ruppert, and SSCD Working Group, Three-dimensional crustal structure of the southern Sierra Nevada from seismic fan profiles and gravity modeling, *Geology, 24*, 367–370, 1996.

Fuis, G. S., and W. D. Mooney, Lithospheric structure and tectonics from seismic-refraction and other data, in *The San Andreas Fault System, California,* edited by R. E. Wallace, *U.S. Geol. Surv. Prof. Pap., P 1515,* 207–236, 1990.

Godfrey, N. J., and S. L. Klemperer, Ophiolitic basement to a forearc basin and implications for continental growth: The Coast Range/Great Valley ophiolite, California, *Tectonics, 17,* 558–570, 1998.

Godfrey, N. J., B. C. Beaudoin, S. L. Klemperer, and Mendocino Working Group, Ophiolitic basement to the Great Valley forearc basin, California, from seismic and gravity data: Implications for crustal growth at the North American continental margin, *Geol. Soc. Am. Bull., 108*, 1536–1562, 1997.

Holbrook, W. S., and W. D. Mooney, The crustal structure of the axis of the Great Valley, California, from seismic refraction measurements, *Tectonophysics, 140,* 49–63, 1987.

Holbrook, W. S., W. D. Mooney, and N. I. Christensen, The seismic velocity structure of the deep continental crust, in *Continental Lower Crust,* edited by D. M. Fountain, R. Arculus, and R. W. Kay, pp. 1–43, Elsevier Sci., New York, 1992.

Hole, J. A., Nonlinear high-resolution three-dimensional seismic travel time tomography, *J. Geophys. Res., 97*, 6553–6562, 1992.

Hole, J. A., and B. C. Zelt, 3-D finite-difference reflection traveltimes, *Geophys. J. Int., 121,* 427–434, 1995.

Hole, J. A., R. M. Clowes, and R. M. Ellis, Interface inversion using broadside seismic refraction data and three-dimensional travel time calculations, *J. Geophys. Res., 97*, 3417–3429, 1992.

Howie, J. M., K. C. Miller, and W. U. Savage, Integrated crustal structure across the south central California margin: Santa Lucia escarpment to the San Andreas Fault, *J. Geophys. Res., 98*, 8173–8196, 1993.

Jachens, R. C., and A. Griscom, An isostatic residual gravity map of California: A residual map for interpretation of anomalies from intracrustal sources, in *The Utility of Regional Gravity and Magnetic Anomaly Maps,* edited by W. J. Hinze, pp. 347–360, Soc. of Explor. Geophys., Tulsa, Okla., 1985.

James, E. W., Cretaceous metamorphism and plutonism in the Santa-Cruz Mountains, Salinian Block, California, and correlation with the southernmost Sierra-Nevada, *Geol. Soc. Am. Bull., 104,* 1326–1339, 1992.

Jones, C. H., and R. A. Phinney, Seismic structure of the lithosphere from teleseismic converted arrivals observed at small arrays in the southern Sierra Nevada and vicinity, California, *J. Geophys. Res., 103*, 10,065–10,090, 1998.

Jones, C. H., H. Kanamori, and S. W. Roecker, Missing roots and mantle "drips": Regional P_n and teleseismic arrival times in the southern Sierra Nevada and vicinity, California, *J. Geophys. Res., 99*, 4567–4601, 1994.

Kistler, R. W., and Z. E. Peterman, Variations in Sr, Rb, K, Na and initial $^{87}Sr/^{86}Sr$ in Mesozoic granitic rocks and intruded wallrocks in central California, *Geol. Soc. Am. Bull., 84*, 3489–3512, 1973.

Kistler, R. W., and Z. E. Peterman, Reconstruction of crustal blocks of California on the basis of initial strontium isotopic compositions of Mesozoic granitic rocks, *U.S. Geol. Surv. Prof. Pap., 1071,* 17 pp., 1978.

Klemperer, S. L., T. A. Hague, E. C. Hauser, J. E. Oliver, and C. J. Potter, The Moho in the northern Basin and Range province, Nevada, along the COCORP 40N seismic-reflection transect, *Geol. Soc. Am. Bull., 97,* 603–618, 1986.

Lachenbruch, A. H., Preliminary geothermal model of the Sierra Nevada, *J. Geophys. Res., 73,* 6977–6989, 1968.

Malin, P. E. et al., Project combines seismic and magnetotelluric surveying to address the Sierran root question, *Eos Trans. AGU, 76*(30), 297–298, 1995.

Miller, D. J., and N. I. Christensen, Seismic signature and geochemistry of an island arc: A multidisciplinary study of the Kohistan accreted terrane, northern Pakistan, *J. Geophys. Res., 99*, 11623–11642, 1994.

Miller, K. C., and W. D. Mooney, Crustal structure and composition of the southern Foothills Metamorphic Belt, Sierra Nevada, California, from seismic data, *J. Geophys. Res., 99*, 6865–6880, 1994.

Mooney, W. D., and C. S. Weaver, Regional crustal structure and tectonics of the Pacific Coastal States; California, Oregon, and Washington, in *Geophysical Framework of the Continental United States,* edited by L. C. Pakiser

and W. D. Mooney, *Mem. Geol. Soc. Am., 172*, 129–161, 1989.

Murphy, J. M., and A. W. Walter, Data report for a seismic-refraction investigation: Morro Bay to the Sierra Nevada, California, *U.S. Geol. Surv. Open File Rep., 84-642*, 39 pp., 1984.

Nicolas, A., F. Boudier, and A. M. Boullier, Mechanisms of flow in naturally and experimentally deformed peridotites, *Am. J. of Sci., 273*, 853–876, 1973.

Oliver, H. W., J. G. Moore, and R. F. Sikora, Internal structure of the Sierra Nevada batholith based on specific gravity and gravity measurements, *Geophys. Res. Lett., 20*, 2179–2182, 1993.

Park, S. K., B. Hirasuna, G. R. Jiracek, and C. Kinn, Magnetotelluric evidence of lithospheric mantle thinning beneath the southern Sierra Nevada, *J. Geophys. Res., 101*, 16,241–16,255, 1996.

Peselnick, L., J. P. Lockwood, and R. Stewart, Anisotropic elastic velocities of some upper mantle xenoliths underlying the Sierra Nevada batholith, *J. Geophys. Res., 82*, 2005–2010, 1977.

Pickett, D. A., and J. B. Saleeby, Thermobarometric constraints on the depth of exposure and conditions of plutonism and metamorphism at deep levels of the Sierra Nevada batholith, Tehachapi Mountains, California, *J. Geophys. Res., 98*, 609–629, 1993.

Rapp, R. P., and E. B. Watson, Dehydration melting of metabasalt at 8–32-kbar: Implications for continental growth and crust-mantle recycling, *J. of Petrol., 36*, 891–931, 1995.

Ruppert, S., M. M. Fliedner, and G. Zandt, Thin crust and active upper mantle beneath the Southern Sierra Nevada in the western United States, *Tectonophysics, 286*, 237–252, 1998.

Saltus, R. W., and A. H. Lachenbruch, Thermal evolution of the Sierra Nevada: tectonic implications of new heat flow data, *Tectonics, 10*, 325–344, 1991.

Saltus, R. W., and G. A. Thompson, Why is it downhill from Tonopah to Las Vegas?: A case for mantle plume support of the high northern Basin and Range, *Tectonics, 14*, 1235–1244, 1995.

Savage, M. K., L. Li, J. P. Eaton, C. H. Jones, and J. N. Brune, Earthquake refraction profiles of the root of the Sierra Nevada, *Tectonics, 13*, 803–817, 1994.

Scott, L., and N. I. Christensen, Upper mantle seismic anisotropy under the Sierra Nevada batholith, California: A xenolith study (abstract), *Eos Trans. AGU, 77*(17), Spring Meet. Suppl., S270, 1996.

Sung, L.-Y., and D. Jackson, Crustal and upper mantle structure under southern California, *Bull. Seismol. Soc. Am., 82*, 934–961, 1992.

Taylor, S. R., and S. M. McLennan, The geochemical evolution of the continental crust, *Rev. Geophys., 33*(2), 241–265, 1995.

Vidale, J. E., Finite-difference calculation of traveltimes in three dimensions, *Geophysics, 55*, 521–526, 1990.

Wentworth, C. M., and M. D. Zoback, Structure of the Coalinga area and thrust origin of the earthquake, in *The Coalinga, California, Earthquake of May 2 1983*, edited by M. J. Rymer and W. L. Ellsworth, *U.S. Geol. Surv. Prof. Pap., 1487*, 41–68, 1990.

Wernicke, B., R. Clayton, M. Ducea, C. H. Jones, S. Park, S. Ruppert, J. Saleeby, J. K. Snow, L. Squires, M. Fliedner, G. Jiracek, R. Keller, S. Klemperer, J. Luetgert, P. Malin, K. Miller, W. Mooney, H. Oliver, and R. Phinney, Origin of High Mountains in the Continents: The Southern Sierra Nevada, *Science, 271*, 190–193, 1996.

Whidden, K. J., S. P. Lund, D. J. Bottjer, D. Champion, and D. G. Howell, Paleomagnetic evidence that the central block of Salinia (California) is not a far-traveled terrane, *Tectonics, 117*, 329–343, 1998.

Zandt, G., A. A. Velasco, and S. L. Beck, Composition and thickness of the southern Altiplano crust, Bolivia, *Geology, 22*, 1003–1006, 1994.

Zelt, B. C., R. M. Ellis, R. M. Clowes, and J. A. Hole, Inversion of three-dimensional wide-angle seismic data from the southwestern Canadian Cordillera, *J. Geophys. Res., 101*, 8503–8529, 1996.

N. I. Christensen, Department of Geology and Geophysics, University of Wisconsin, 1215 W. Dayton Street, Madison, WI 53706. (e-mail: chris@geology.wisc.edu)

M. M. Fliedner, Bullard Laboratories, University of Cambridge, Madingley Road, Cambridge CB3 0EZ, England. (email: moritz@esc.cam.ac.uk)

S. L. Klemperer, Department of Geophysics, Stanford University, Stanford, CA 94305-2215. (e-mail: sklemp@geo.stanford.edu)

(Received May 20, 1999; revised November 22, 1999; accepted January 12, 2000.)